Links between memory, synapses, amyloid-beta, tau and microglial changes after tau pathology induction by Alzheimer's brain inoculation in amyloid-beta-plaque bearing mice

Suzanne Lam[1,2], Anne-Sophie Hérard[1,2], Susana Boluda[3,4],
Fanny Petit[1,2], Sabiha Eddarkaoui[5], Karine Cambon[1,2],
The Brainbank Neuro-CEB Neuropathology Network[4,§], Jean-Luc Picq[1,2,6],
Luc Buée[5], Charles Duyckaerts[3,4], Stéphane Haïk[3,4], Marc Dhenain[1,2]

Author affiliations:

[1] Université Paris-Saclay, CEA, CNRS, Laboratoire des Maladies Neurodégénératives, 18 Route du Panorama, F-92265 Fontenay-aux-Roses, France.

[2] Commissariat à l'Energie Atomique et aux Energies Alternatives (CEA), Direction de la Recherche Fondamentale (DRF), Institut François Jacob, MIRCen, 18 Route du Panorama, F-92265 Fontenay-aux-Roses, France

[3] ICM Institut du Cerveau et de la Moelle épinière, CNRS UMR7225, INSERM U1127, Sorbonne Université, Hôpital de la Pitié-Salpêtrière, Paris, France.

[4] Brainbank NeuroCEB Neuropathology Network: Plate-Forme de Ressources Biologiques, Bâtiment Roger Baillet, Hôpital de la Pitié-Salpêtrière, 47-83 boulevard de l'Hôpital, 75651 Paris Cedex 13.

[5] Université de Lille, Inserm, CHU-Lille, Lille Neuroscience & Cognition, Alzheimer & Tauopathies, LabEx DISTALZ, Rue Polonovski, 59045 Lille, France.

[6] University Paris 8, Laboratory of Cognitive Functioning and Dysfunctioning (DysCo), Saint-Denis 93526 cedex, France.

Correspondence to: Marc Dhenain, DVM, PhD
Université Paris-Saclay, CEA, CNRS, Laboratoire des Maladies Neurodégénératives, MIRCen, 18 Route du Panorama, F-92265 Fontenay-aux-Roses, France
E-mail: marc.dhenain@cea.fr

Abstract

Background:

Alzheimer's disease (AD) is characterized by the presence of both extracellular amyloid-β (Aβ) plaques and intracellular tau accumulations. The causative interactions between these lesions, and the subsequent neuroinflammation, synaptic alterations and memory impairment are still debated. Intracerebral infusion of human AD brain extracts in Aβ bearing mice that do not overexpress pathological tau proteins induces widespread Aβ and tau pathologies following heterotopic seeding of mouse tau. These models provide a unique opportunity to assess relationships between AD lesions and downstream events.

Methods:

Human AD and control-brain extracts (AD_{be} and $Ctrl_{be}$) were infused in the hippocampus of Aβ plaque-bearing $APP_{swe}/PS1_{dE9}$ mice. We evaluated the links between Aβ plaques, tau aggregates, microgliosis, astrogliosis at the inoculation site and in connected regions (perirhinal/entorhinal cortex), and memory impairment and synaptic density 4 and 8 months post-inoculation.

Results:

AD_{be}-inoculated animals displayed memory deficit and synaptic loss in addition to Aβ and tau pathological aggregates. Aβ plaques were detected in both AD_{be}- and $Ctrl_{be}$-inoculated $APP_{swe}/PS1_{dE9}$ mice, but their load was increased close to the inoculation site in AD_{be}-inoculated animals. Tau-positive neuropil threads and neurofibrillary tangles occurred next to the inoculation site only in AD_{be}-inoculated animals and were not detected in $Ctrl_{be}$ mice. These lesions spread to connected regions notably the perirhinal/entorhinal cortex. Tau-positive neuritic plaques were detected in both AD_{be}- and $Ctrl_{be}$-inoculated animals. Unexpectedly, AD_{be} inoculation did not increase the number of neuritic plaques close to the inoculation site as compared to $Ctrl_{be}$ inoculation. AD_{be} inoculation however increased the area of tau-positive

elements within these neuritic plaques. Increased tau pathology as well as lower Iba1-positive microglial load in the hippocampus and perirhinal/entorhinal cortex were correlated with memory impairment and with synaptic loss.

Conclusions:

The integrative analysis of pathological events associated with AD_{be} inoculation in Aβ-bearing mice highlighted memory and synaptic loss as well as the induction of tau lesions that spread in the brain. Increased tau lesions and lower microglial load are the two main events correlated with memory impairment and synaptic loss. The study suggests that microglial activity may be protective.

Keywords

Alzheimer's disease; Amyloid-β, memory, microglia; synapses; tau; transmission

Graphical abstract

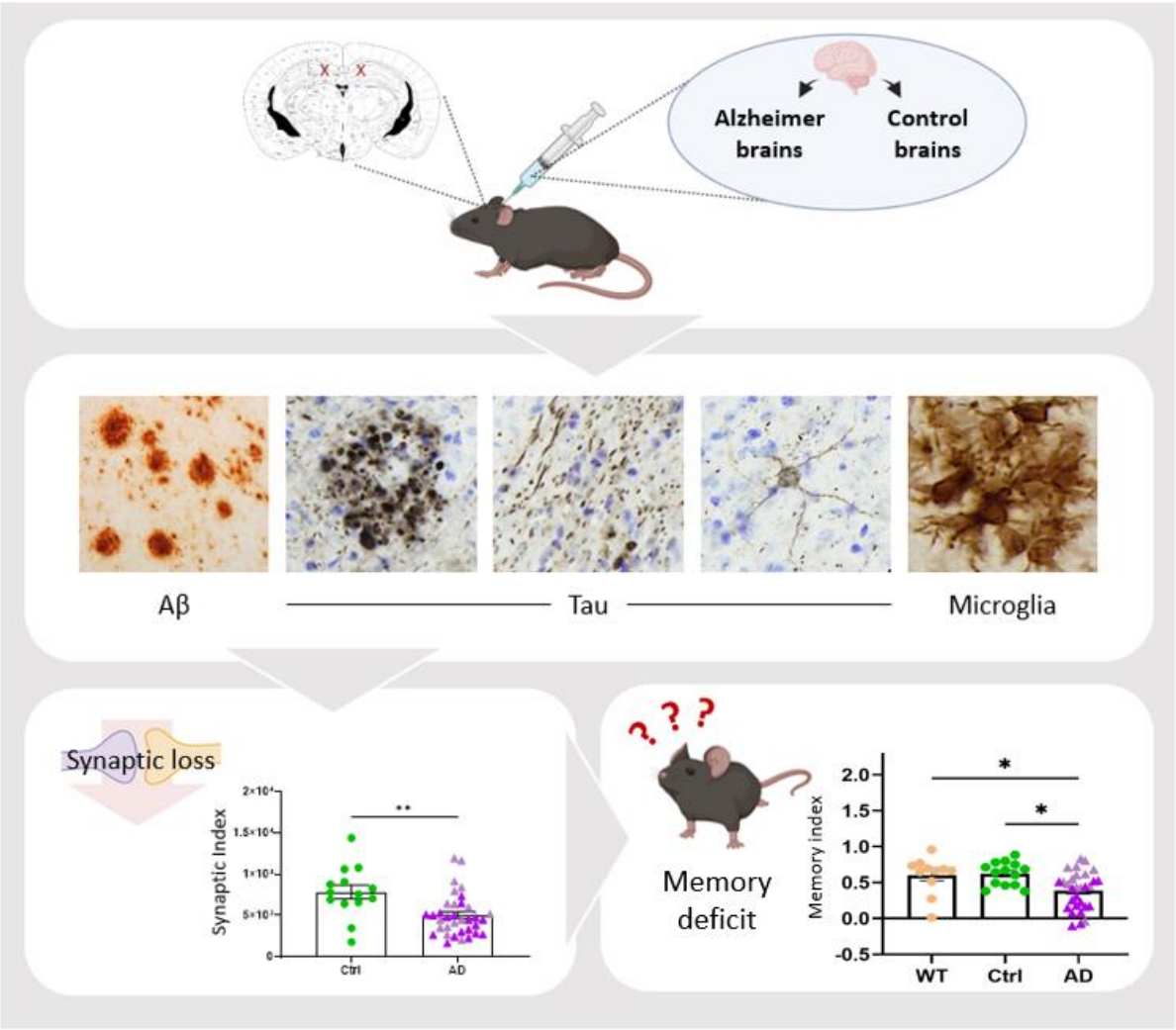

Background

Amyloid-β (Aβ) plaques and intracellular tau accumulations are two of the cerebral lesions that define the neuropathological diagnosis of Alzheimer's disease (AD). Intracellular tau accumulations spread in a highly stereotyped pattern throughout the brain [1]. These lesions engender neuroinflammation including microgliosis [2] and synaptic alterations [3]. The etiologic link between Aβ-proteopathy and tauopathy in AD and their role in memory loss remains largely undefined.

In humans, memory impairment is correlated with synaptic deficits [3] and with neocortical tau pathology but not as well with Aβ plaque load [4, 5]. Transgenic (Tg) mice overexpressing human Aβ or tau (with or without frontotemporal dementia mutations) were used to further elucidate the interactions between Aβ, tau and synaptic or memory impairments. Previous studies in Tg models overexpressing Aβ highlighted associations between memory or synaptic deficits and Aβ pathology [6-8]. Additionally, studies in Tg models overexpressing tau protein also highlighted associations between memory or synaptic deficits and tau pathology [8-11]. These results suggest a role of both Aβ and tau pathologies in the induction of memory or synaptic deficits in rodents.

Microglia are other key regulators of AD pathophysiology. In humans, genetic evidence exemplified by the lower incidence of AD in individuals with loss-of-function Trem2 mutations that impair microglial activation [12], suggested that microglia have a protective function. In non-genetic cases of AD, some studies [13], but not all [14], outline the potential protective function of microglia. There are evidence in several mouse models with genetic-related microglial impairment (*e.g.* Trem2 deficient mice) [15, 16] or with microglia depletion [17, 18] that suggest that microglial activation is protective. However, other studies in mice have shown that microglial activation can be toxic for synapses in Aβ-plaque bearing models [19] as well

as in mice overexpressing human tau as microglia can engulf tau-positive synapses [11, 20]. Thus the role of microglia in AD pathology remains to be elucidated.

AD is characterized by both Aβ and tau pathologies and as such it remains critical to investigate any relationship between AD markers in animal models presenting with both Aβ and tau lesions. Mouse models of amyloidosis were shown to display tau lesions mainly in neurites close to Aβ deposits [21-23]. Presumably due to the low level of tau pathology in these animals, they are not used as models of both Aβ and tau pathologies. Tg mice overexpressing both human mutated Aβ and tau were developed to further assess interactions between Aβ and tau pathologies and their impact on brain function [24]. One of the limitations of these models is the overexpression in a non-physiological manner of both mutated Aβ and tau, which depends in part, on the gene promoter used [25]. To bypass these models, new protocols were recently established to reproduce both Aβ and tau pathologies in a single model via the intracerebral infusion of human AD brain extracts (AD_{be}) in Aβ bearing mice that do not overexpress pathological tau proteins [26, 27]. These protocols rely on the notion that tau proteins have prion-like properties and can be experimentally transmitted. Once in the cell environment, they can be taken up by unaffected cells, and are amplified by seeding the aggregation of endogenous tau. Tau pathologies occur in AD_{be}-inoculated transgenic Aβ-bearing mice due to tau proteins from AD_{be} that induce the heterotopic seeding of mouse tau [27, 28]. These models were mainly used to investigate the relationships between Aβ and tau pathologies [15, 26, 27]. They display memory impairment, however, the relationships between AD core lesions and downstream events including synaptic and memory changes remain mostly undefined in these models [26, 27]. Investigation into these questions is key for further use of these models to untangle AD pathophysiology and potential relevant therapies. To address these questions, we infused Alzheimer's disease (AD_{be}) as well as control brain extracts ($Ctrl_{be}$) in the hippocampus of $APP_{swe}/PS1_{dE9}$ mice that have a high Aβ production, express the endogenous murine tau protein

isoforms and are not transgenic for any human tau. Mice inoculated with AD_{be} displayed memory impairment and synaptic loss. They had increased Aβ load at the inoculation site, increased tau lesions that spread in connected areas notably the perirhinal/entorhinal cortex. Tau lesions were correlated with memory defects and with synaptic loss. Memory impairment and synaptic loss were also associated with lower microglial load.

Methods

Human brain collection, characterization, and brain extract preparation

Frozen brain samples (parietal cortex) from clinically different sporadic AD patients (four patients with classical slowly evolving forms and four with a rapidly evolving forms of AD) as well as two age-matched control individuals were collected from a brain donation program of the NeuroCEB and the CNR-prion brain banks (Supplementary Table 1). Consent forms were previously signed by either the patients themselves or their next of kin, in accordance with French bioethics laws. The classical slowly evolving AD cases (AD1) were characterized by a disease duration of 5 to 8 years. The rapidly evolving AD cases (AD2) were characterized by a disease duration of 6 months to 3 years. No case of hippocampal sclerosis was reported and all brain samples were PrPSc negative. Samples from AD brains were also negative for α-synuclein and TDP-43. The characterization by immunohistochemistry of Aβ plaques and tau lesions of all brain tissues used in this study is reported in [29]. Parietal cortex samples from each patient were individually homogenized at 10% weight/volume (w/v) in a sterile 1X Dulbecco's phosphate buffer solution in CK14 soft tissue homogenizing tubes at 5000 rpm for 20 sec (Precellys®, Bertin technologies). They were then sonicated on ice for 5 sec at 40% amplitude and centrifuged at 3000g for 5 min at +4°C. The resulting supernatant was aliquoted in sterile polypropylene tubes and stored at − 80 °C until use. Ten percent Ctrl, AD1 or AD2 individual

brain extracts were thawed on ice and combined together according to their group. Aβ levels, total tau and phospho-tau181 as well as Iba1 and GFAP protein levels were assessed by biochemistry in each brain extract. Their characteristics are published in [29]. The amounts of Aβ, tau and neuroinflammatory proteins differed slightly between the brain extracts, as the AD2 extract displayed more total tau and phospho-tau181, but less $A\beta_{38}$ and $A\beta_{40}$ than the AD1 one. Iba1 and GFAP levels were similar in the two AD extracts.

Transgenic mice

Mouse experiments used the $APP_{swe}/PS1_{dE9}$ mouse model of amyloidosis (C57Bl6 background) [30]. Aβ plaques can be detected as early as 4 months of age in these mice, and increase in number and total area with age [30]. This model expresses endogenous murine tau protein isoforms and is not transgenic for any human tau. At the time of the inoculation of AD or Ctrl brain extracts in their brains, at 2 months of age, these mice did not have Aβ plaques. Animals were studied four or eight months after intracerebral inoculation of the brain extracts (at 4 and 8 months post-inoculation (mpi) respectively, n_{Ctrl}=11 and 15, n_{AD1}=14 and 15, n_{AD2}=12 and 20). Wild-type littermates injected with the Ctrl brain sample were used as controls for the behavioral tests (at 4 and 8 mpi respectively, n_{WT}=6 and 12). A cohort of 21 animals were studied by immunohistochemistry one month post-inoculation (n_{Ctrl}=6, n_{AD1}=7, n_{AD2}=8). All $APP_{swe}/PS1_{dE9}$ mice were born and bred in our center (Commissariat à l'Energie Atomique, centre de Fontenay-aux-Roses; European Institutions Agreement #B92-032-02). All animals were randomly assigned to the experimental groups using a simple procedure: they were identified using increasing numbers based on their birthdate. Animals with increasing numbers were alternatively assigned to the Ctrl (animal 1, 4, 7…), AD1 (animal 2, 5, 8…) and AD2 groups (animal 3, 6, 9…). Males were exclusively used in this study in order to optimize group homogeneity (as Aβ plaque load varies between males and females). Mice were injected during different inoculation sessions and each group was randomly inoculated at each session to avoid

an "order of treatment" confounding effect. All experimental procedures were conducted in accordance with the European Community Council Directive 2010/63/UE and approved by local ethics committees (CEtEA-CEA DSV IdF N°44, France) and the French Ministry of Education and Research (A17_083 authorization given after depositing the research protocol and associated ethic issues), and in compliance with the 3R guidelines. Animal care was supervised by a dedicated in-house veterinarian and animal technicians. Humane endpoints concerning untreatable continuous suffering signs and prostrations were taken into account and not reached during the study. Animals were housed under standard environmental conditions (12-h light-dark cycle, temperature: 22 ± 1°C and humidity: 50%) with *ad libitum* access to food and water. The design and reporting of animal experiments were based on the ARRIVE reporting guidelines [31]. Sample size choice was based on previous experiments for Aβ induction in $APP_{swe}/PS1_{dE9}$ mice after inoculation of human brain (n = 8 at 4 mpi estimated with significance level of 5%, a power of 80%, and a two-sided test) [32] and increased to take into account uncertainties for new markers (tau lesion load, memory and synaptic changes). No animals were excluded from the study. SL was aware of initial group allocation, but further analyses (memory evaluations and post-mortem studies) were performed blinded.

Stereotaxic surgery

Ten percent Ctrl, AD1 and AD2 brain extracts were thawed on ice. Extracts were then pooled together according to their group and the three resulting combined samples ($Ctrl_{be}$, $AD1_{be}$, $AD2_{be}$) were sonicated (70% amplitude, 10 sec on/off; Branson SFX 150 cell disruptor sonicator, 3.17mm microtip probe Emerson, Bron) on ice in a sterile environment, extemporaneously before stereotaxic injection.

Two month-old $APP_{swe}/PS1_{dE9}$ and wild-type littermates were anesthetized by an intraperitoneal injection of ketamine (1mg/10g; Imalgène 1000, Merial) and xylazine (0.1mg/10g; 2% Rompun, Bayer Healthcare). Local anesthesia was also performed by a

subcutaneous injection of lidocaine at the incision site (1 µl/g; 0.5% Xylovet, Ceva). Mice were placed in the stereotaxic frame (Phymep) and bilateral injections of brain samples were performed in the dorsal hippocampus (AP -2 mm, DV -2 mm, L +/- 1 mm from bregma). Using 34-gauge needles and Hamilton syringes, 2µl/site of sample were administered at a 0.2µl/min rate. After the injection, needles were kept in place for 5 more minutes before removal and the incision was sutured. The surgical area was cleaned before and after the procedure using povidone iodine (Vétédine, Vétoquinol). Respiration rate was monitored and body temperature was maintained at 37±0.5°C with a heating pad during the surgery. Anesthesia was reversed with a subcutaneous injection of atipamezole (0.25 mg/kg; Antisedan, Vetoquinol). Mice were placed in a ventilated heating box (25°C) and monitored until full recovery from anesthesia. Postoperative anticipatory pain management consisted in paracetamol administration in drinking water (1.45 ml/20ml of water; Doliprane, Sanofi) during 48 hours.

Behavioral evaluations

A battery of behavorial tests including an elevated plus maze, a novel object recognition task in a V-maze, and a Morris water maze were conducted at 4 mpi or 8 mpi on $Ctrl_{be}$-, $AD1_{be}$-, or $AD2_{be}$-inoculated $APP_{swe}/PS1_{dE9}$ mice. Wild-type littermates injected with the $Ctrl_{be}$ were used as controls for the tests. Mice were handled for 2 minutes per day, for 5 days prior to any test to prevent stress effects during tasks. Prior to each test, mice were habituated to the experimental room for 30 minutes. The experimenter was blind to mouse groups. Performances were recorded using a tracking software (EthoVision XT14, Noldus).

Elevated plus maze

The elevated plus maze is a plus-shaped apparatus placed at 50 cm above the floor. It consists of four 5 cm-wide and 40 cm-long segments, among which two are open arms (associated with a 150 lux-lighting) and two are enclosed arms (associated with a 15 lux-lighting). Mice were

placed at the center of the maze facing an open arm for a 6-min trial. Distance travelled and time spent in each arm were automatically calculated by the software. The time spent leaning over the edge of open arms was scored manually. Between runs, the elevated plus maze was cleaned with 10% ethanol and dried.

Novel object recognition in the V-maze

The V-maze arena consisted in two 6 cm-wide, 33.5 cm-long and 15 cm-high black arms forming a V shape and exposed to a 50 lux-lighting. The test was divided into three phases, each one separated by 24 hours. At the beginning of each session, mice were placed at the center of the arena, *i.e.* at the intersection of the arms. During the habituation phase (day 1), mice were free to explore the empty arena for 9 minutes. The distance travelled was automatically recorded as an indicator of their exploratory activity. For the training phase (day 2), two identical objects (bicolor plastic balls) were placed at the end of each arm. Exploratory activity was evaluated as the time spent exploring the objects (manually recorded) and the distance travelled during the 9-minute trial. On the test day (day 3), one familiar object (a bicolor plastic ball) was replaced by a novel one of a different shape and material (a transparent glass flask). Recognition was assessed using a discrimination index, calculated as follows:

$$Discrimination\ index = \frac{Time\ exploring\ the\ novel\ object - Time\ exploring\ the\ familiar\ object}{Total\ exploration\ time}$$

It reflects the time spent exploring each object, and therefore, the ability to discriminate a novel object from a familiar, previously explored one. A low discrimination index score reveals that mice spent less time exploring the new object, *i.e.* still had marked interest in the familiar object, and suggests that memory was impaired. Between each run, the V-maze was cleaned with 10% ethanol and dried.

Morris water maze

An open 122 cm-wide circular swimming arena with water was maintained at 22°C and exposed to a 400 lux-lighting. A platform put in the swimming arena allow to escape from the water. Visual cues were placed around the maze so that mice could spatially navigate to the platform. The test consisted of three phases during which the arena was divided into four virtual quadrants. At the end of each session, mice were dried with a heated towel before being returned to their home cages. During the habituation phase (day 1), mice were trained to find a visible platform to escape from the water. To facilitate its detection, the platform was emerged 0.5 cm above the surface of the water and a colorful cue was placed on it. This phase consisted of four 60-seconds trials, with an inter-trial interval of 20-30 minutes. For each trial, the starting point was different as well as the location of the platform. When the mice did not find the platform within the 60 seconds time limit, they were guided to its location and were left on the platform to rest for 30 seconds. The training phase (day 2 to 6) consisted in three daily 60-seconds trials, with 20-30 minutes inter-trial interval, for five days. For each trial, the starting point was different whereas the location of the platform remained the same. The platform was hidden 0.5 cm beneath the water surface and the cue previously placed on it was removed. When the mice did not find the platform within 60 seconds, they were guided to its location and were left on the platform to rest for 30 seconds. All trials lasted 60 seconds or until the animal located the platform. Escape latency, *i.e.* the time required to find the platform, was evaluated during the habituation and the training phases to assess learning abilities. A probe test (day 7) was performed 72 hours after the last training session to assess spatial long-term memory. During this phase, the platform was removed from the maze. Mice were placed in the water for 60 seconds from a position opposite to the hidden platform. The time spent in each virtual quadrant of the maze was recorded.

Animal euthanasia and brain preparation for histology

Mice were sacrificed at 4 or 8 mpi, after the behavioural tests, with an intraperitoneal injection of a lethal dose of pentobarbital (100 mg/kg; Exagon, Axience). They were perfused intracardiacally with cold sterile 0.1M PBS for 4 minutes, at a rate of 8 ml/min. The brain was extracted and post-fixed in 4% paraformaldehyde for 48 hours at +4°C, transferred in a 15% sucrose solution for 24 hours and in a 30% sucrose solution for 48 hours at +4°C for cryoprotection. Serial coronal sections of 40 µm were performed with a microtome (SM2400, Leica Microsystem) and stored at -20°C in a storing solution (glycerol 30%, ethylene glycol 30%, distilled water 30%, phosphate buffer 10%). Free-floating sections were rinced in a 0.1M PBS solution (10% Sigma-Aldrich® phosphate buffer, 0.9% Sigma-Aldrich® NaCl, distilled water) before use. Washing and incubation steps were performed on a shaker at room temperature unless indicated otherwise.

Immunohistochemistry for Aβ, tau, microglia and astroglia

Aβ deposits were evaluated using a 4G8 labelling. Tau was evaluated using labelling with AT8 directed against hyperphosphorylated tau and AT100 that binds to a conformational epitope including phosphorylated Thr212 and Ser214. Microglia were evaluated using Iba1 and CD68 antibodies. Astrocytes were stained with the GFAP antibody.

4G8 labelling was performed after pretreating brain sections with 70% formic acid (VWR®) for 20 min at room temperature. AT8 and AT100 labellings were performed after a pretreatment with EDTA 1X citrate (Diagnostic BioSystems®) for 30 min at 95°C. All tissues were then incubated in hydrogen peroxide H_2O_2 30% (Sigma-Aldrich®) diluted 1/100 for 20 min to inhibit endogenous peroxidases. Blocking of non-specific antigenic sites was achieved over 1 hour using a 0.2% Triton X-100/0.1M PBS (Sigma-Aldrich®) (PBST) solution containing 4.5% normal goat serum or 5% bovine serum albumin. Sections were then incubated at +4°C with

the 4G8 (Biolegend 800706, 1/500), Iba1 (Wako 1919741, 1/1000), CD68 (Serotec – Biorad MCA 1957, 1/800) or GFAP (Dako Z0334, 1/10000) antibody diluted in a 3%NGS/PBST solution for 48h, or with the AT8 (Thermo MN1020B, 1/500) or AT100 (Thermo MN1060, 1/500) antibody diluted in a 3%NGS/PBST solution for 96h. After rinsing, an incubation with the appropriate biotinylated secondary antibody diluted to 1/1000 in PBST was performed for 1h at room temperature, followed by a 1h incubation at room temperature with a 1:250 dilution of an avidin-biotin complex solution (ABC Vectastain kit, Vector Laboratories®). Revelation was performed using the DAB Peroxidase Substrate Kit (DAB SK4100 kit, Vector Laboratories®). Sections were mounted on Superfrost Plus slides (Thermo-Scientific®). For the AT8 and AT100 labellings, a cresyl violet counterstain was performed. All sections were then dehydrated in successive baths of ethanol at 50°, 70°, 96° and 100° and in xylene. Slides were mounted with the Eukitt® mounting medium (Chem-Lab®).

Stained sections were scanned using an Axio Scan.Z1 (Zeiss® - Z-stack images acquired at 20× (z-stacks with 16 planes, 1µm steps with extended depth of focus)). Each slice was extracted individually in the .czi format using the Zen 2.0 (Zeiss®) software. Image processing and analysis were performed with the ImageJ software. Macros were developed for each staining in order to attain a reproducible semi-automated quantification. Images were imported with a 50% reduction in resolution (0.44 µm/pixel), converted to the RGB format and compressed in .Tif format. For the 4G8, Iba1 and CD68 immunostainings, segmentation was performed through an automatic local thresholding using the Phansalkar method (radius = 15). Aβ load was evaluated after quantification of the 4G8-labelled particles between 8 and 2,000 µm², and normalization to the surface area of each ROI. Microglial status was evaluated as a percentage of Iba1- or CD68-positive surface area in each ROI. For the AT8 and AT100 stainings, the blue component of each image was extracted to remove the cresyl violet counter-staining from the analysis. AT8-positive or AT100-positive tau loads were assessed following an automatic local

thresholding of the staining with the Phansalkar method followed by an evaluation of the percentage of AT8-positive or AT100-positive surface area in each ROI.

In general, tau lesions occur in the form of neuropil threads, neurofibrillary tangles (NFTs), and neuritic plaques *i.e.* tau aggregates within neurites surrounding Aβ deposits. In addition for the AT8 immunostaining, a quantification of neuritic plaques and NFTs was performed by manual counting. The AT8-positive area stained within neuritic plaques was evaluated by drawing circular regions of interest (with a constant area of 6µm²), and by quantifying the percentage of tau-positive regions within each ROI, using the same thresholding method as previously described. A semi-quantitative analysis of neuropil threads was also performed by assigning a severity score based on the intensity and extent of AT8-positive staining in each ROI. All quantifications were performed on adjacent slices between -0.34 mm and -4.36 mm from bregma. Ten adjacent slices were analyzed for the 4G8 staining, and 5 for Iba1, CD68, AT8, and AT100 stainings. All ROIs were manually segmented using the Paxinos and Franklin neuro-anatomical atlas of mouse brain [33].

Gallyas silver staining

Free-floating sections were mounted on Superfrost Plus (Thermo-Scientific®) slides and dried overnight prior to Gallyas staining. Section were permeabilized by successive incubations in toluene (2x5min) followed by ethanol at 100°, 90° and 70° (2 min per solution). Slides were then incubated in a 0.25% potassium permanganate solution for 15 min, in 2% oxalic acid for 2 min then in a lanthanum nitrate solution (0.04g/l lanthanum nitrate, 0.2g/l sodium acetate, 10% H2O2 30%) for 1h to reduce non-specific background. Several rinses with distilled water were performed followed by an incubation in an alkaline silver iodide solution (3.5% AgNO3 1%, 40g/l NaOH, 100g/l KI) for 2 min. The reaction was neutralized with 0.5% glacial acetic acid baths (3x1min) and sections were incubated for 20 min in a developing solution (2g/l NH4NO3, 2g/l AgNO3, 10g/l tungstosilicilic acid, 0.76% formaldehyde 37%, 50g/l anhydrous

Na2CO3). Several rinses with 0.5% acetic acid (3x1min) followed by an incubation in 1% gold chloride solution for 5min were then carried out. Sections were rinsed with distilled water and the staining was fixed with a 1% sodium thiosulfate solution. All sections were then rinsed with distilled water and dehydrated for 1 to 5 min in successive baths of ethanol at 50°, 70°, 96° and 100° and in xylene. Slides were mounted with the Eukitt® mounting medium (Chem-Lab®). All steps were performed at room temperature.

Co-stainings of microglia and Aβ plaques

In order to evaluate microglial load surrounding Aβ plaques, the co-staining of microglia and Aβ plaques was performed. Free-floating sections were permeabilized in a 0.2% Triton X-100/0.1M PBS (Sigma-Aldrich®) solution for 3x10min. Slices were stained by MXO4 dye (Tocris #4920, 1/300) for 30 min at room temperature, and then washed in a 0.1M PBS solution. Sections were blocked in a 4.5%NGS/PBST solution for 1h at room temperature before being incubated with the Iba1 antibody (Wako 1919741, 1/1000). Twenty four hours later, sections were rinsed in 0.1M PBS and incubated for 1h at room temperature with the appropriate secondary antibody diluted to 1/1000 in PBST (anti-rabbit AlexaFluor 633). Sections were rinsed and mounted on Superfrost Plus (Thermo-Scientific®) slides with the Vectashield® mounting medium with a refractive index of 1.45. Images of stained sections were acquired using a Leica DMI6000 confocal optical microscope (TCS SPE) with a 40x oil-immersion objective (refractive index 1.518) and the Leica Las X software. A confocal zoom of 3 and a pinhole aperture fixed at 1 Airy were applied. Acquisition was performed in sequential mode with a sampling rate of 1024x1024 and a scanning speed of 700 Hz. Image resolution was 60 nm/pixel and the optical section was 0.896 µm. Twelve separate planes with a 0.1 µm step were acquired. The excitation wavelengths were 633 nm (for Iba1) or 350 nm (for Aβ). Image acquisition was performed on 2 slices located between -3.28 mm and -4.24 mm from the bregma, with 3 images per slice for the CA1 region and for the perirhinal/entorhinal cortex. 3D

deconvolution of the images was performed using the AutoQuant X3 software. The deconvoluted 8-bit images were analyzed using the ImageJ software. Quantification of microglial load around plaques was based on a thresholding procedure applied across all images to segment microglial cells. MXO4-positive surfaces were dilated as circular regions of interest (with a diameter of 40 µm) were drawn around the Aβ plaque to define a dilated plaque area. Microglial staining within the dilated surface, *e.g.* within the plaque area, was included in the analysis.

Evaluation of synaptic density

Synaptic density was evaluated in the hippocampus (CA1) and the perirhinal/entorhinal cortex of all inoculated mice using a double immunolabelling of presynaptic (Bassoon) and postsynaptic (Homer1) markers. Free-floating sections were permeabilized in a 0.5% Triton X-100/0.1M PBS (Sigma-Aldrich®) solution for 15min. Slices were incubated with Bassoon (Abcam Ab82958, 1/200) and Homer1 (Synaptic systems 160003, 1/400) antibodies diluted in 3% BSA/PBST solution for 24 hours at +4°C. Incubation with secondary antibodies coupled to a fluorochrome (Alexa Fluor) diluted in a 3% BSA/0.1M PBS solution was then performed for 1h at room temperature. Sections were rinsed and mounted on Superfrost Plus (Thermo-Scientific®) slides with the Vectashield® mounting medium with a refractive index of 1.45. Images of stained sections were acquired using a Leica DMI6000 confocal optical microscope (TCS SPE) with a 63x oil-immersion objective (refractive index 1.518) and the Leica Las X software. A confocal zoom of 3 and a pinhole aperture fixed at 1 Airy were applied. Acquisition was performed in sequential mode with a sampling rate of 1024 x 1024 and a scanning speed of 700 Hz. Image resolution was 60 nm/pixel and the optical section was 0.896 µm. 26 separate planes with a 0.2 µm step were acquired. The excitation wavelengths were 594 nm or 633 nm. Image acquisition in the CA1 region was performed on 4 adjacent slices located between -1.82 mm and -3.28 mm from the bregma, with 2 images per slice. For the perirhinal/entorhinal

cortex, 3 adjacent slices located between -3.28 mm and -4.24 mm from the bregma were analyzed, with 2 images acquired per slice. 3D deconvolution of the images was performed using the AutoQuant X3 software. The deconvoluted 8-bit images were analyzed using the ImageJ software, as described in Gilles et al [34]. Briefly, automated 3D segmentation of the staining allowed to determine the volume occupied by Bassoon-positive or Homer-positive objects in the 3D space as well as the localization of the geometrical centroid or center of mass of the objects. Co-localization was determined by the detection of overlapping objects, and depended on the center-to-center distance and the percentage of co-localization volumes for each pair of objects.

Statistical analysis

Statistical analysis was performed using the GraphPad Prism software 8. Data from AD1 and AD2 mice were pooled within a single AD_{be}-inoculated group. For the behavioral tasks analysis, Kruskal-Wallis tests with Dunn's multiple comparisons were perfomed except when repeated measures were acquired, in which case, a two-way repeated measures ANOVA with the Geisser-Greenhouse correction and Dunnett's multiple comparisons was carried out. Wilcoxon's signed-rank test was used to compare the time spent in the Morris Water maze quadrants with the theoretical value of 15 seconds (25% of trial duration). For the post-mortem analysis, Mann-Whitney tests were performed in order to compare differences between AD_{be}-inoculated (AD1 and AD2 mice) and $Ctrl_{be}$-inoculated mice . For correlation studies, Spearman correlation test was performed. The significance level was set at $p<0.05$. Data are shown on scattered dot plots with mean ± standard error of the mean (s.e.m).

Data availability

The data that support the findings of this study are available from the corresponding author, upon request.

Results

AD_{be}-inoculated Aβ transgenic mice develop memory alteration

AD_{be} and $Ctrl_{be}$ were inoculated bilaterally in the dorsal hippocampus (CA1) of 2-month-old $APP_{swe}/PS1_{dE9}$ mice. An additional group of $Ctrl_{be}$-inoculated wild-type littermates was used as a control. Inoculated mice were evaluated using a battery of behavioral tests at 8 mpi.

First, the mice were evaluated in an object-recognition task (V-maze test). Animals from each group showed similar exploratory activity, as suggested by similar distance travelled throughout the three days of test (Fig. 1A) and comparable interest in the two identical objects during the training phase of the task (Fig. 1B). During the memory task, *i.e.* the novel object recognition evaluation, $Ctrl_{be}$-inoculated wild-type and $APP_{swe}/PS1_{dE9}$ mice had similar performances (Fig. 1C). Compared to these two groups, AD_{be}-inoculated $APP_{swe}/PS1_{dE9}$ mice spent less time exploring the novel object, which is a marker of memory impairment, (Fig. 1C). Spatial memory was then assessed using the Morris water maze test (Supplementary Fig. 1A-C). During the training phase, no difference was observed between the groups suggesting that $Ctrl_{be}$ and AD_{be} inoculations do not differentially impact spatial learning abilities in $APP_{swe}/PS1_{dE9}$ mice (Supplementary Fig. 1A-B). Spatial memory was then evaluated 72 hours after the last training test. All groups performed as well as the wild-type group by spending more time in the target quadrant than in the opposite one, suggesting that spatial memory is not impaired in $Ctrl_{be}$- or AD_{be}-inoculated $APP_{swe}/PS1_{dE9}$ mice (Supplementary Fig. 1C). Moreover, the time spent both in the target quadrant and in the opposite one was significantly different from the theoretical value of 15 seconds, which corresponds to 25% of the trial duration, supporting the idea that all groups successfully memorized the platform location (Supplementary Fig. 1C).

Anxiety levels were evaluated using the general aversion of rodents to open spaces in the elevated plus maze test. The different groups did not display differences in the distance

travelled, the time spent leaning over the maze, as well as the time spent in open and enclosed arms or at their intersection in the center of the arena (Supplementary Fig. 1D-F). These results suggest that anxiety levels at 8 mpi are neither impacted by the $APP_{swe}/PS1_{dE9}$ genotype, nor by the intracerebral AD_{be} inoculation.

Another cohort of mice was also evaluated at 4 mpi (n_{Ctrl}=11, n_{AD1}=14, n_{AD2}=12, n_{WT}=6). No difference in memory performance was observed at this stage (Supplementary Fig. 2A-C).

AD_{be}-inoculated mice display decreased synaptic density

Synaptic density was decreased by 19% in the CA1 of the hippocampus (Fig. 1D) and by 36% in the perirhinal/entorhinal cortex (Fig. 1E) of AD_{be}-inoculated mice compared to $Ctrl_{be}$ mice at 8 mpi. The memory index in the V-maze was correlated with synaptic defects in the CA1 (Fig. 1F) but not in the perirhinal/entorhinal cortex (Fig. 1G). Synaptic density changes were not detected at 4 mpi (Supplementary Fig. 2D-E).

Increased Aβ plaque deposition and tau pathologies close to the infusion site in AD_{be}-inoculated mice

At 8 mpi, AD_{be} infusion led to a statistically significant increase in Aβ plaque deposition in the hippocampus and in the region surrounding the alveus compared to $Ctrl_{be}$ (Fig. 2). Similar changes were found at 4 mpi (Supplementary Fig. 2F-G). This suggests that the increase in Aβ pathology detected at 8 mpi already started at 4 mpi.

AD_{be}-inoculated $APP_{swe}/PS1_{dE9}$ mice developed AT8-positive neuritic plaques (NPs) (Fig. 3A, G-I), neuropil threads (NTs) (Fig. 3B) and NFTs (Fig. 3C-F) at 4 and 8 mpi. At 1 mpi, tau lesions were not detected in any animal (Supplementary Fig. 3).

Neuritic plaques were also detected in the hippocampus of $Ctrl_{be}$-inoculated $APP_{swe}/PS1_{dE9}$ mice at 8 mpi (Fig. 3G) while other tau-positive lesions were not detected in $Ctrl_{be}$-inoculated $APP_{swe}/PS1_{dE9}$ mice. We performed an AT8 immunostaining on old non-inoculated

$APP_{swe}/PS1_{dE9}$ mice and also observed neuritic plaques (Fig. 3J). This suggests that AD_{be} inoculation is not necessary to induce tau lesions in neuritic plaques. Quantitative analysis showed that neuritic plaque count in the hippocampus was similar in AD_{be}- and $Ctrl_{be}$-inoculated mice (Fig. 3K). The AT8-positive area stained within neuritic plaques was however larger in the AD_{be}-inoculated groups compared to $Ctrl_{be}$ animals (Fig. 3G-I and 3L).

Further quantitative analysis at 8 mpi showed that, compared to the $Ctrl_{be}$-inoculated mice, AD_{be}-inoculated animals displayed an increase in AT8-positive tau lesions in the hippocampus (Fig. 3M-O, 3S) and in the alveus (Fig. 3P-R, 3T). These increases of AT8-positive tau lesions were already reported at 4 mpi, although to a lesser extent (Supplementary Fig. 2I-J).

Unlike AD_{be}-inoculated $APP_{swe}/PS1_{dE9}$ mice, $Ctrl_{be}$-inoculated animals did not present AT8-positive neuropil threads or NFTs. Thus logically, AT8-positive neuropil threads were increased both in the hippocampus (Fig. 3U) and the alveus (Fig. 3V) of AD_{be}-inoculated mice as compared to $Ctrl_{be}$-inoculated animals. Also AT8-positive NFTs were increased in the hippocampus of AD_{be}-inoculated mice compared to $Ctrl_{be}$-inoculated (Fig. 3W). AT8-positive NFTs were not present in the alveus of any animals (not shown).

Further evaluation of tau lesions revealed AT100 positive labelling in the forms of neuropil threads and NFTs (Supplementary Fig. 4A), in both groups of AD_{be}-inoculated mice. Quantification of the AT100 staining showed increased labelling in the alveus of AD_{be}-inoculated mice but not in the hippocampus (Supplementary Fig. 4B-C). Gallyas silver staining revealed neuropil thread labelling (Supplementary Fig. 4D), as well as Aβ plaques (Supplementary Fig. 4E). No quantification was performed as this technique reveals both tau and Aβ pathologies.

Spreading of tau pathology in AD_{be}-inoculated mice

We then evaluated Aβ and tau pathologies in the perirhinal/entorhinal brain regions that are connected to the hippocampus (Fig. 4A-B). Aβ load was similar in the perirhinal/entorhinal

cortex of AD_{be}- and $Ctrl_{be}$-inoculated $APP_{swe}/PS1_{dE9}$ mice at 8 mpi (Fig. 4C-E, 4I) or at 4 mpi (Supplementary Fig. 2H). Aβ detected in the perirhinal/entorhinal cortex may thus only reflect the endogenous expression of the peptide in the $APP_{swe}/PS1_{dE9}$ model.

Conversely, overall AT8-positive areas of tau lesions were clearly increased in the perirhinal/entorhinal cortex of AD_{be}-inoculated animals compared to $Ctrl_{be}$-inoculated ones (Fig. 4F-H, 4J). Also, both the number of neuritic plaques, and the AT8-positive area stained within neuritic plaques were increased in the perirhinal/entorhinal cortex of AD_{be}-inoculated mice compared to $Ctrl_{be}$ mice (Fig. 4K-L). Neuropil threads and NFTs were detected in the perirhinal/entorhinal cortex of AD_{be}-inoculated mice but not in $Ctrl_{be}$-inoculated animals (Fig. 4M-N). All tau lesions were mainly found in the external layers II and III of the cortex (Fig 4F-H) that project to the dentate gyrus via the perforant pathway and to the CA1 region via the temporo-ammonic pathway, respectively. On the contrary, internal layers (*e.g.* layers V-VI) that receive projections from the CA1 region were not labelled. Other cortical regions such as the visual cortex also displayed neuropil threads, NFTs and neuritic plaques in AD_{be}-inoculated mice (Supplementary Fig. 5A-B).

As in the hippocampus, AT100 staining revealed tau lesions in the perirhinal/entorhinal cortex (Supplementary Fig. 6A-B), and a statistical difference in AT100-positive staining was detected between the AD_{be} and $Ctrl_{be}$ groups (Supplementary Fig. 6C). Gallyas staining was also positive for tau lesions (Supplementary Fig. 6D-E) and Aβ plaques (Supplementary Fig. 6D and 6F) in this region.

Tau lesion load in AD_{be}- and $Ctrl_{be}$-inoculated mice were not different in the perirhinal/entorhinal cortex at 4 mpi (Supplementary Fig. 2K). This result should be compared with the reported increased level of tau lesions in AD_{be}-inoculated mice next to the inoculation site (Supplementary Fig. 2I-J) and the increased presence of tau lesions at both sites at 8 mpi in

AD_{be}-inoculated mice. It suggests that tau pathology gradually spreads to the perirhinal/entorhinal cortex in a time-dependent manner from 4 to 8 mpi.

Neuroinflammatory response

Neuroinflammation was assessed by staining brain tissues using Iba1, a general marker for microglia as well as an anti-CD68 antibody that stains a lysosomal protein expressed at high levels by activated microglia and at low levels by resting microglia. Iba1 staining was positively correlated with CD68 staining in the hippocampus and the perirhinal/entorhinal cortex (Supplementary Fig. 7A-B). Visual observation of the stained sections suggested different levels of staining for Iba1 with some animals displaying high Iba1 labelling (Fig. 5A-B) and some others lower staining (Fig. 5E-F). Animals displaying high Iba1 labelling showed abundant activated microglia characterized by beading with spheroidal swellings of the processes and enlarged cell body with dystrophic ramifications (Fig. 5C, arrows) [35]. These activated cells formed microglial clusters surrounding Aβ plaques (Fig. 5D). In contrast, mice with low Iba1 labelling (Fig. 5E-F) displayed highly ramified microglia, both close to and far from Aβ plaques (Fig. 5G and 5H respectively), which is consistent with a non-activated phenotype. Quantification revealed similar levels of Iba1 (Fig. 5M-N) and CD68 (Fig. 5O-P) stained areas in the hippocampus or perirhinal/entorhinal cortex of AD_{be} and $Ctrl_{be}$ groups ($p>0.05$). Microglial activation was proposed to shield Aβ plaques off from neurons to prevent their toxicity [17]. Using confocal microscopy, we showed that, as expected, Iba1-stained microglia surrounding Aβ plaques (Supplementary Fig. 7C). As for Iba1, some animals displayed high CD68 labelling (Fig. 5I) and some others lower staining (Fig. 5J). Some clusters of CD68-stained microglia surrounded Aβ deposits (Fig. 5K) while some others were not associated with Aβ deposits (Fig. 5L). We thus evaluated whether microglial load surrounding Aβ plaques differed following the inoculation of various brain extracts. We could not detect

any differences in Iba1 staining around plaques in the different groups (Fig. 5Q-R). This suggests no difference in the shielding effect in our inoculated groups.

Finally, astrocyte reactivity (GFAP staining) was evaluated and no difference was detected between the groups in the hippocampus and in the perirhinal/entorhinal cortex (Supplementary Fig. 8).

Memory score is correlated with increased tau and Aβ loads and decreased synaptic density

Memory score in the V-maze was correlated with synaptic density (Fig. 1F-G) and inversely correlated with tau pathology in both the hippocampus and the connected perirhinal/entorhinal cortex (AT8-positive tau load (Fig. 6A-B), AT8-positive area stained within neuritic plaques (Fig. 6C-D), neuropil threads (Fig. 6E-F), NFTs (Fig. 6G-H)). It was also inversely correlated with Aβ load in the hippocampus, but not in the perirhinal/entorhinal cortex (Fig. 7A-B). Finally, it was positively correlated with microglial load stained by Iba1 in the hippocampus and perirhinal/entorhinal cortex (Fig. 7C-D) but not with CD68 staining (Fig. 7E-F). No relationship between memory score and astrocyte-associated GFAP staining was observed (not shown).

Synaptic density is associated with tau pathology and reduced microglial activation but not with Aβ plaque load

Synaptic density in the hippocampus (CA1) and in the perirhinal/entorhinal cortex was inversely correlated with AT8-positive tau load in the same region (Fig. 8A, 8E). Synaptic density in the perirhinal/entorhinal cortex was inversely correlated with neuritic plaque count (Fig. 8F), AT8-positive area stained within neuritic plaques (Fig. 8G), neuropil threads (Fig. 8H), and NFTs (Fig. 8I). Synaptic density was not correlated with Aβ load in the hippocampus nor in the perirhinal/entorhinal cortex (Fig. 8B, 8J). A positive correlation was also reported

between synaptic density and Iba1 staining in the hippocampus (Fig. 8C) and between synaptic density and Iba1 (Fig. 8K) or CD68 stainings (Fig. 8L) in the perirhinal/entorhinal cortex. This suggests that microglial activation is associated with higher synaptic density. No relationship between synaptic density and astrocyte-associated GFAP staining was observed in these regions (not shown).

Discussion

We used a strategy based on the intracerebral infusion of AD_{be} into $APP_{swe}/PS1_{dE9}$ Aβ-bearing mice to induce tau lesions that spread in the brain, increase Aβ pathology close to the inoculation site, and induce downstream events including memory impairment and reduction of synaptic density (Supplementary Fig. 9). As compared to previous studies in similar models [26, 27], our study proposed an integrative analysis to explore downstream events, including synaptic and memory changes, associated with induced lesions (Supplementary Fig. 10).

In humans, tau lesions occur in the form of neuritic plaques *i.e.* tau aggregates within neurites surrounding Aβ deposits, as well as neuropil threads and NFTs. These three forms of tau aggregates were detected in AD_{be}-inoculated animals. But only neuritic plaques were detected in $Ctrl_{be}$-inoculated animals as well as in aged non-inoculated $APP_{swe}/PS1_{dE9}$ mice. Previous studies have shown that the forms of tau induced by AD_{be} infusion are characteristic of mouse tau and not human tau and suggested that human tau favor the heterotopic seeding of mouse tau [27, 28]. In our study, the lack of tau detection at one month post-inoculation and its progressive occurrence thereafter, is consistent with the hypothesis that tau detected at 4 months and later does not reflect a direct deposit of tau from ADbe and suggest that deposition arises from mouse tau.

The presence of neuritic plaques in $Ctrl_{be}$-inoculated animals and non-inoculated mice suggests that Aβ aggregates, *per se*, are sufficient to induce tau lesions in surrounding neurites leading to neuritic plaques. This hypothesis is consistent with an increasing number of reports showing

neuritic plaques in $APP_{swe}/PS1_{dE9}$ mice [23] or in other Aβ-bearing Tg mice [21, 22]. In humans, different lesions with amyloid structure, including non-Aβ prion plaques, can also induce neuritic tau lesions [36], which further extends the concept that amyloid lesions favor neuritic tau pathology.

Unexpectedly, the number of neuritic plaques was not increased at the inoculation site in AD_{be}-inoculated animals as compared to $Ctrl_{be}$-inoculated ones. The only difference between AD_{be} and $Ctrl_{be}$-inoculated groups concerned the density of tau lesions within neuritic plaques which was higher in AD_{be}-inoculated animals. These results could suggest that AD_{be} are not the main inducer of neuritic plaques, even if they could increase their severity.

Unlike neuritic plaques, neuropil threads and NFTs were only induced in AD_{be}-inoculated animals. Previous studies have suggested that neuropil threads and NFTs occur secondarily to the presence of tau seeds issued from neuritic plaques [26]. We cannot totally rule out that an increased level of tau within neuritic plaques could be a source of tau to induce neuropil threads or NFTs. However, based on the presence of neuropil threads and NFTs only in AD_{be}-inoculated animals, we hypothesize that AD_{be} are the main source of seeds for tau induction and spreading in neuropil threads and NFTs. Consistent with this hypothesis, in a previous study, we induced neuropil threads and NFTs but not neuritic plaques in primates by infusing the AD_{be} used in the currend study [29].

Tau pathology (AT8-positive tau load, neuritic plaque counts, AT8-positive area stained within neuritic plaques, neuropil threads, and NFTs in the hippocampus and in the perirhinal/entorhinal cortex, *i.e.* at distance from the inoculation site) were correlated with memory alterations at 8 mpi. In addition, tau pathology was correlated with synaptic deficits in the hippocampus (CA1) and the perirhinal/entorhinal cortex. These results, in a model that is not based on tau overexpression, strongly supports the hypothesis that tau pathology contributes to synaptic loss. As memory alterations at 8 mpi were correlated with synaptic loss in the hippocampus, tau-

associated synaptic loss can be one of the factors mediating the relationship between memory impairment and tau pathology.

Memory evaluations did not show any difference between $Ctrl_{be}$-inoculated wild-type and Aβ-bearing mice at 8 mpi, *i.e.* at an age when Aβ plaques are numerous in the mice. Also, the severity of Aβ load in the perirhinal/entorhinal cortex in AD_{be}- and $Ctrl_{be}$-inoculated $APP_{swe}/PS1_{de9}$ mice at 8 mpi was not associated with memory changes. This suggests a limited effect of Aβ plaques on memory at 8 mpi. This hypothesis would be consistent with the weak association between synaptic loss and Aβ plaque load at this age. We however, noticed that memory alterations at 8 mpi were associated with the severity of Aβ load in the hippocampus. Tau pathology, which was also correlated with Aβ load in this region, was also correlated with memory changes. Thus, we think that the apparent relationship between Aβ pathology in the hippocampus and memory reflects the effect of tau pathologyt. As Aβ and tau have been proposed to interact to induce memory changes [37], it is also possible that increasing tau pathology in mice increased Aβ toxicity. Further studies will have to be designed to further evaluate the role of Aβ and in particular, the soluble forms of Aβ in AD_{be}-inoculated Aβ-bearing mice.

Microglia is the last lesion evaluated in our study. Although we did not detect differences of microglia load in AD_{be} and $Ctrl_{be}$-inoculated animals, we took advantage of interindividual heterogeneity to assess the relationships between microglia load and memory changes or synaptic density. The correlation between memory alterations and lower Iba1-positive microglial load in the hippocampus and perirhinal/entorhinal cortex *i.e.* at distance from the inoculation site suggests a protective effect of microglia activation. Additionally, synaptic loss was correlated with a reduction of microgliosis in the hippocampus (for Iba1 staining), or in the perirhinal/entorhinal cortex (for both Iba1 and CD68 stainings). This further reinforces a potential protective effect of microglial activation in, for the first time, a mouse model without

genetic or chemical manipulation of microglia. Microglia activation could be protective for synapses and thus protect from deleterious memory changes due to brain extracts inoculations in mice.

Conclusions

We showed that the intracerebral infusion of AD_{be}- into Aβ plaque–bearing mice that do not overexpress tau can increase Aβ and tau pathologies and lead to downstream events including memory impairment and reduction of synaptic density. Tau lesions were correlated with memory defects and with reduction of synaptic density. This latter can be one of the factors mediating the relationship between memory impairment and tau pathology. Memory impairment and synaptic loss were also associated with lower microglial load. This suggests a protective effect of microglial activity and supports the impetus to engage in further studies to assess the potential negative impacts of anti-inflammatory therapies targeting microglia in subjects at risk for AD. Finally, our integrative pathophysiological analysis of a novel model with Aβ plaques, induced tau pathology that spread in the brain as well as memory and synaptic impairments, *i.e.* an outcome highly relevant to AD pathology, is critical for the future use of this model for candidate drug evaluations.

List of abbreviations

Aβ = amyloid-β; AD = Alzheimer's disease; AD1 = slowly evolving form of Alzheimer; AD2 = rapidly evolving form of Alzheimer; AD_{be} = AD brain extracts; Ctrl = control; $Ctrl_{be}$ = control brain extracts; mpi = months post-inoculation; NFTs = neurofibrillary tangles; NP = neuritic plaques; NT = neuropil threads; WT = wild-type.

Declarations

Ethics approval and consent to participate

All experimental procedures were conducted in accordance with the European Community Council Directive 2010/63/UE and approved by local ethics committees (CEtEA-CEA DSV IdF N°44, France) and the French Ministry of Education and Research (A17_083 authorization given after depositing the research protocol and associated ethic issues), and in compliance with the 3R guidelines. Animal care was supervised by a dedicated veterinarian and animal technicians. Humane endpoints concerned untreatable continuous suffering signs and prostrations were used and not reached during the study.

Consent for publication

Does not apply to the content of this article.

Availability of data and materials

The data that support the findings of this study are available from the corresponding author, upon reasonable request.

Competing interests

The authors declare that they have no competing interests.

Funding

The project was funded by the Association France-Alzheimer. It was performed in a core facility supported by/member of NeurATRIS - ANR-11-INBS-0011. It was also supported by internal funds from the Laboratory of Neurodegenerative Diseases and MIRCen. SL was financed by the French Ministère de l'Enseignement Supérieur, de la Recherche, et de

l'Innovation. She was also financed by the Fondation pour la Recherche Médicale. The funding sources had no role in the design of the study, in the collection, analysis, and interpretation of data, nor in writing the manuscript.

Atuhor's contributions

S.L., A.S.H., F.P., and M.D. contributed to the study conception and design. N.N.N., C.D. provided the human brain samples. N.N.N., S.L., S.B., C.D. and S.H. characterized the human brain samples. S.L., M.G. and M.G. performed the inoculations in mice. S.L. and K.C. designed and performed memory evaluations, A.S.H., F.P., and S.L. designed and performed the immunohistological analysis in animals. A.S.H., S.E., L.B., and S.L. performed biochemical analysis. S.L., A.S.H., and M.D. wrote the manuscript. All authors commented on previous versions of the manuscript. All authors read and approved the final manuscript.

Acknowledgements

We thank Martine Guillermier and Mylène Gaudin for surgical expertise during inoculation of brain extracts to animals. We thank Nicolas Heck for his help in synapse quantification, and Cecilia Garrec for the editing and English language correction, and Nicolas Sergeant for a critical review of this article. We thank the donors and the Brain Donation Program of the NeuroCEB Brainbank Neuropathologist's Network run by a consortium of Patient Associations: ARSLA (association for research on amyotrophic lateral sclerosis), CSC (cerebellar ataxias), Fondation ARSEP (association for research on multiple sclerosis), France DFT (fronto-temporal dementia), Fondation Vaincre Alzheimer, France Parkinson, with the support of Fondation Plan Alzheimer and IHU A-ICM for providing the brain samples used in this study. NeuroCEB Brainbank Neuropathologit's Network members: Franck Letournel (Angers), Marie-Laure Martin-Négrier (Bordeaux), Maxime Faisant (Caen), Catherine Godfraind (Clermont-Ferrand), Jean Boutonnat (Grenoble), Claude-Alain Maurage (Lille),

Vincent Deramecourt (Lille), Mathilde Duchesne (Limoges), David Meyronet (Lyon), Tanguy Fenouil (Lyon), André Mauès de Paula (Marseille), Valérie Rigau (Montpellier), Fanny Vandenbos-Burel (Nice), Danielle Seilhean (Paris), Charles Duyckaerts (Paris), Susana Boluda (Paris), Isabelle Plu (Paris), Dan Christian Chiforeanu (Rennes), Annie Laquerrière (Rouen), Florent Marguet (Rouen), Béatrice Lannes (Strasbourg), Benoît Lhermitte (Strasbourg).

REFERENCES

1. Braak H, Braak E. Neuropathological stageing of Alzheimer related changes. Acta Neuropathol 1991; 82(4): 239-59. https://doi.org/10.1007/BF00308809.

2. Hansen DV, Hanson JE, Sheng M. Microglia in Alzheimer's disease. J Cell Biol 2018; 217(2): 459-72. https://doi.org/10.1083/jcb.201709069.

3. Terry RD, Masliah E, Salmon DP, Butters N, DeTeresa R, Hill R*, et al.* Physical basis of cognitive alterations in Alzheimer's disease: synapse loss is the major correlate of cognitive impairment. Ann Neurol 1991; 30(4): 572-80. https://doi.org/10.1002/ana.410300410.

4. Nelson PT, Alafuzoff I, Bigio EH, Bouras C, Braak H, Cairns NJ*, et al.* Correlation of Alzheimer disease neuropathologic changes with cognitive status: a review of the literature. J Neuropath Exp Neur 2012; 71(5): 362-81. https://doi.org/10.1097/NEN.0b013e31825018f7.

5. Bennett DA, Schneider JA, Wilson RS, Bienias JL, Arnold SE. Neurofibrillary tangles mediate the association of amyloid load with clinical Alzheimer disease and level of cognitive function. Arch Neurol 2004; 61(3): 378-84. https://doi.org/10.1001/archneur.61.3.378.

6. Selkoe DJ. Alzheimer's disease is a synaptic failure. Science 2002; 298(5594): 789-91. https://doi.org/10.1126/science.1074069.

7. Sivanesan S, Tan A, Rajadas J. Pathogenesis of abeta oligomers in synaptic failure. Curr Alzh Res 2013; 10(3): 316e23. https://doi.org/10.2174/1567205011310030011.

8. Spires-Jones TL, Hyman BT. The intersection of amyloid beta and tau at synapses in Alzheimer's disease. Neuron 2014; 82(4): 756-71. https://doi.org/10.1016/j.neuron.2014.05.004.

9. Hoover BR, Reed MN, Su J, Penrod RD, Kotilinek LA, Grant MK*, et al.* Tau mislocalization to dendritic spines mediates synaptic dysfunction independently of neurodegeneration. Neuron 2010; 68(6): 1067-81. https://doi.org/10.1016/j.neuron.2010.11.030.

10. Pooler AM, Noble W, Hanger DP. A role for tau at the synapse in Alzheimer's disease pathogenesis. Neuropharmacology 2014; 76: 1-8. https://doi.org/10.1016/j.neuropharm.2013.09.018.

728 11. Dejanovic B, Huntley MA, De Maziere A, Meilandt WJ, Wu T, Srinivasan K*, et al.* Changes in the
729 synaptic proteome in tauopathy and rescue of Tau-induced synapse loss by C1q antibodies. Neuron
730 2018; 100(6): 1322-36.e7. https://doi.org/10.1016/j.neuron.2018.10.014.
731 12. Dourlen P, Kilinc D, Malmanche N, Chapuis J, Lambert JC. The new genetic landscape of Alzheimer's
732 disease: from amyloid cascade to genetically driven synaptic failure hypothesis? Acta Neuropathol
733 2019; 138(2): 221-36. https://doi.org/10.1007/s00401-019-02004-0.
734 13. Streit WJ, Braak H, Xue QS, Bechmann I. Dystrophic (senescent) rather than activated microglial
735 cells are associated with tau pathology and likely precede neurodegeneration in Alzheimer's disease.
736 Acta Neuropathol 2009; 118(4): 475-85. https://doi.org/10.1007/s00401-009-0556-6.
737 14. Perez-Nievas BG, Stein TD, Tai HC, Dols-Icardo O, Scotton TC, Barroeta-Espar I*, et al.* Dissecting
738 phenotypic traits linked to human resilience to Alzheimer's pathology. Brain 2013; 136: 2510-26.
739 https://doi.org/10.1093/brain/awt171.
740 15. Leyns CEG, Gratuze M, Narasimhan S, Jain N, Koscal LJ, Jiang H*, et al.* TREM2 function impedes tau
741 seeding in neuritic plaques. Nat Neurosci 2019; 22(8): 1217-22. https://doi.org/10.1038/s41593-019-
742 0433-0.
743 16. Lee S-H, Meilandt WJ, Xie L, Gandham VD, Ngu H, Barck KH*, et al.* Trem2 restrains the enhancement
744 of tau accumulation and neurodegeneration by b-amyloid pathology. Neuron 2021; 109(8): 1283–
745 301.e6. https://doi.org/10.1016/j.neuron.2021.02.010.
746 17. Condello C, Yuan P, Schain A, Grutzendler J. Microglia constitute a barrier that prevents neurotoxic
747 protofibrillar Abeta42 hotspots around plaques. Nat Commun 2015; 6: 6176.
748 https://doi.org/10.1038/ncomms7176.
749 18. Clayton K, Delpech JC, Herron S, Iwahara N, Ericsson M, Saito T*, et al.* Plaque associated microglia
750 hyper-secrete extracellular vesicles and accelerate tau propagation in a humanized APP mouse model.
751 Mol Neurodegener 2021; 16: Article number 18. Erratum in: Mol Neurodegener. 2021;16(1):24.
752 https://doi.org/10.1186/s13024-021-00440-9.

753 19. Spangenberg EE, Lee RJ, Najafi AR, Rice RA, Elmore MRP, Blurton-Jones M*, et al.* Eliminating
754 microglia in Alzheimer's mice prevents neuronal loss without modulating amyloid-beta pathology.
755 Brain 2016; 139: 1265-81. https://doi.org/10.1093/brain/aww016.
756 20. Leyns CEG, Ulrich JD, Finn MB, Stewart FR, Koscal LJ, Serrano JR*, et al.* TREM2 deficiency attenuates
757 neuroinflammation and protects against neurodegeneration in a mouse model of tauopathy. Proc Natl
758 Acad Sci USA 2017; 114(43): 11524-9. https://doi.org/10.1073/pnas.1710311114.
759 21. Noda-Saita K, Terai K, Iwai A, Tsukamoto M, Shitaka Y, Kawabata S*, et al.* Exclusive association and
760 simultaneous appearance of congophilic plaques and AT8-positive dystrophic neurites in Tg2576 mice
761 suggest a mechanism of senile plaque formation and progression of neuritic dystrophy in Alzheimer's
762 disease. Acta Neuropathol 2004; 108(5): 435-42. https://doi.org/10.1007/s00401-004-0907-2.
763 22. Radde R, Bolmont T, Kaeser SA, Coomaraswamy J, Lindau D, Stoltze L*, et al.* Abeta42-driven cerebral
764 amyloidosis in transgenic mice reveals early and robust pathology. EMBO reports 2006; 7(9): 940-6.
765 https://doi.org/10.1038/sj.embor.7400784.
766 23. Metaxas A, Thygesen C, Kempf SJ, Anzalone M, Vaitheeswaran R, Petersen S*, et al.* Ageing and
767 amyloidosis underlie the molecular and pathological alterations of tau in a mouse model of familial
768 Alzheimer's disease. Sci Rep 2019; 9(1): Article number 15758. https://doi.org/10.1038/S41598-019-
769 52357-5.
770 24. Oddo S, Caccamo A, Shepherd JD, Murphy MP, Golde TE, Kayed R*, et al.* Triple-transgenic model of
771 Alzheimer's disease with plaques and tangles: intracellular Abeta and synaptic dysfunction. Neuron
772 2003; 39(3): 409-21. https://doi.org/10.1016/s0896-6273(03)00434-3.
773 25. Drummond E, Wisniewski T. Alzheimer's disease: experimental models and reality. Acta
774 Neuropathol 2017; 133(2): 155-75. https://doi.org/10.1007/s00401-016-1662-x.
775 26. He ZH, Guo JL, McBride JD, Narasimhan S, Kim H, Changolkar L*, et al.* Amyloid-beta plaques enhance
776 Alzheimer's brain tau-seeded pathologies by facilitating neuritic plaque tau aggregation. Nat Med
777 2018; 24(1): 29-38. https://doi.org/10.1038/nm.4443.

778 27. Vergara C, Houben S, Suain V, Yilmaz Z, De Decker R, Vanden Dries V*, et al.* Amyloid- pathology
779 enhances pathological fibrillary tau seeding induced by Alzheimer PHF in vivo. Acta Neuropathol 2019;
780 137(3): 397-412. https://doi.org/10.1007/s00401-018-1953-5.
781 28. Audouard E, Houben S, Masaracchia C, Yilmaz Z, Suain V, Authelet M*, et al.* High-molecular-weight
782 paired helical filaments from Alzheimer brain induces seeding of wild-type mouse tau into an
783 argyrophilic 4R Tau pathology in vivo. Am J Pathol 2016; 186(10): 2709-22.
784 https://doi.org/10.1016/j.ajpath.2016.06.008.
785 29. Lam S, Petit F, Hérard A-S, Boluda S, Eddarkaoui S, Guillermier M*, et al.* Transmission of amyloid-
786 beta and tau pathologies is associated with cognitive impairments in a primate. Acta Neuropathol
787 Commun 2021; 9: 165. https://doi.org/10.1186/s40478-021-01266-8.
788 30. Garcia-Alloza M, Robbins EM, Zhang-Nunes SX, Purcell SM, Betensky RA, Raju S*, et al.*
789 Characterization of amyloid deposition in the APPswe/PS1dE9 mouse model of Alzheimer disease.
790 Neurobiol Dis 2006; 24(3): 516-24. https://doi.org/10.1016/j.nbd.2006.08.017.
791 31. du Sert NP, Hurst V, Ahluwalia A, Alam S, Avey MT, Baker M*, et al.* The ARRIVE guidelines 2.0:
792 Updated guidelines for reporting animal research. Bmc Vet Res 2020; 16(1): Article 242.
793 https://doi.org/10.1186/s12917-020-02451-y.
794 32. Gary C, Lam S, Herard AS, Koch JE, Petit F, Gipchtein P*, et al.* Encephalopathy induced by Alzheimer
795 brain inoculation in a non-human primate. Acta Neuropathol Commun 2019; 7(1): 126.
796 https://doi.org/10.1186/s40478-019-0771-x.
797 33. Paxinos G, Franklin KBJ. The mouse brain in stereotaxic coordinates. second ed. San Diego:
798 Academic Press; 2001.
799 34. Gilles JF, Dos Santos M, Boudier T, Bolte S, Heck N. DiAna, an ImageJ tool for object-based 3D co-
800 localization and distance analysis. Methods 2017; 115: 55-64.
801 https://doi.org/10.1016/j.ymeth.2016.11.016.

802 35. Sanchez-Mejias E, Navarro V, Jimenez S, Sanchez-Mico M, Sanchez-Varo R, Nunez-Diaz C*, et al.*
803 Soluble phospho-tau from Alzheimer's disease hippocampus drives microglial degeneration. Acta
804 Neuropathol 2016; 132(6): 897-916. https://doi.org/10.1007/s00401-016-1630-5.
805 36. Duyckaerts C, Sazdovitch V, Ando K, Seilhean D, Privat N, Yilmaz Z*, et al.* Neuropathology of
806 iatrogenic Creutzfeldt-Jakob disease and immunoassay of French cadaver-sourced growth hormone
807 batches suggest possible transmission of tauopathy and long incubation periods for the transmission
808 of Abeta pathology. Acta Neuropathol 2018; 135(2): 201-12. https://doi.org/10.1007/s00401-017-
809 1791-x.
810 37. Roberson ED, Scearce-Levie K, Palop JJ, Yan F, Cheng IH, Wu T*, et al.* Reducing endogenous tau
811 ameliorates amyloid beta-induced deficits in an Alzheimer's disease mouse model. Science 2007;
812 316(5825): 750-4. https://doi.org/10.1126/science.1141736.

FIGURES

FIGURE LEGENDS

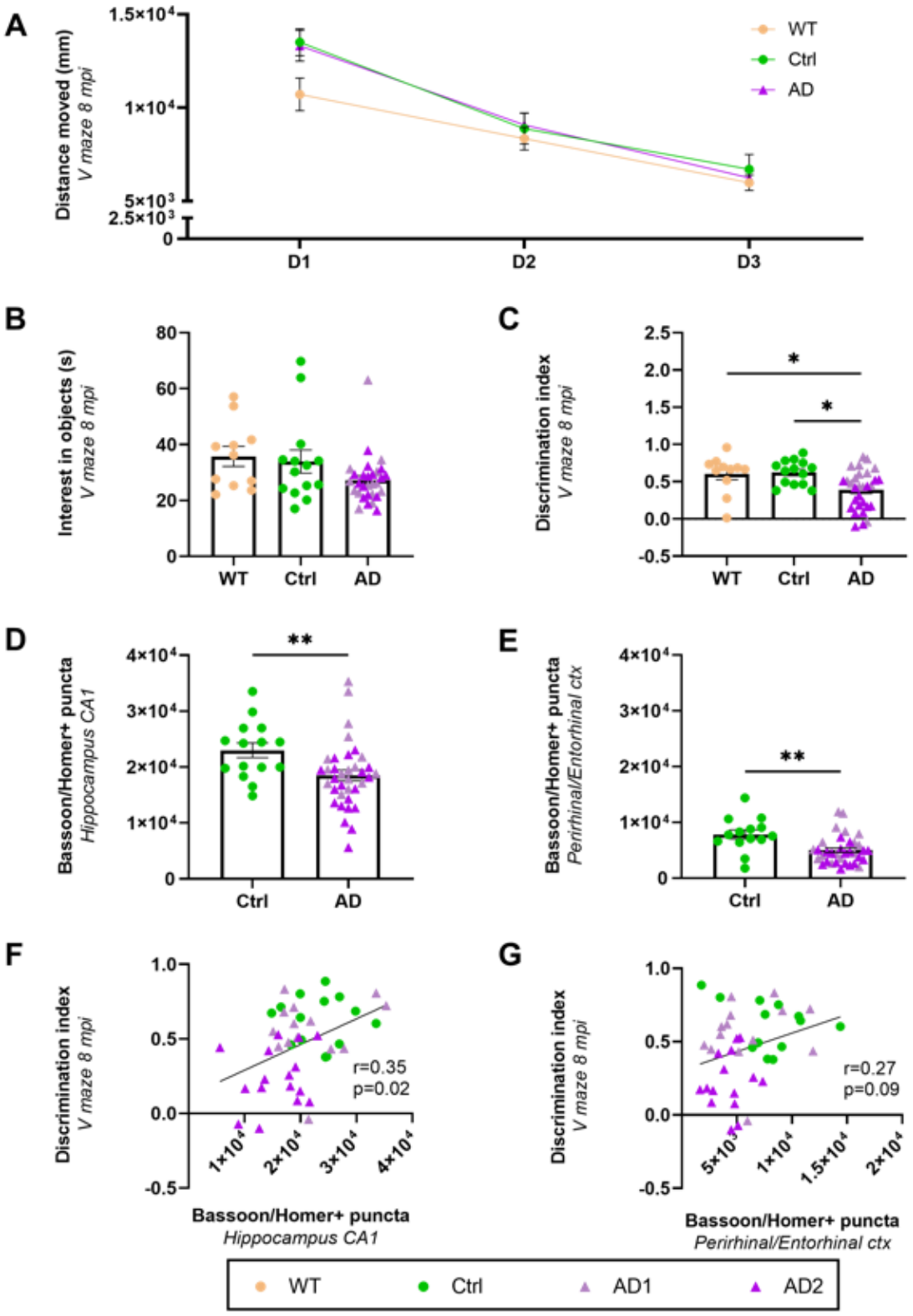

Figure 1. Object recognition deficits and synaptotoxicity in the AD_{be}-inoculated mice. Object recognition performances were evaluated at 8 mpi in a V-maze. WT mice and $APP_{swe}/PS1_{dE9}$ mice inoculated with $Ctrl_{be}$ or AD_{be} had comparable exploratory activity, as suggested by the distance moved throughout the 3-day test (**A**, for the days: $F_{(1.7, 90.5)} = 72.4$, $p<0.0001$; for the groups: $F_{(2, 52)} = 1.2$, $p=0.3$; two-way repeated measures ANOVA with the Geisser-Greenhouse correction and Dunnett's multiple comparisons) and the time spent on exploring the objects (**B**, $p>0.05$; Kruskal-Wallis with Dunn's multiple comparisons). During the novel object recognition evaluation, AD_{be}-inoculated mice spent less time exploring the novel object, as suggested by a lower discrimination index, compared to WT and $APP_{swe}/PS1_{dE9}$ $Ctrl_{be}$-inoculated mice (**C**, respectively, $p=0.027$, and 0.016; Kruskal-Wallis with Dunn's multiple comparisons). (**D**-**E**) Quantification of Bassoon and Homer colocalization revealed a decrease in synaptic density in AD_{be} mice in the CA1 (**D**, Mann Whitney's test, U=137, $p=0.005$) and perirhinal/entorhinal cortex (**E**, Mann Whitney's test, U=109, $p=0.002$), compared to $Ctrl_{be}$-inoculated mice at 8 mpi. V-maze memory scores (discrimination index) were correlated with synaptic defects in the CA1 (**F**, $r_{hip}=0.35$, p=0.02) but not in the perirhinal/entorhinal cortex (**G**, $r_{P/EC}=0.27$, $p=0.29$). $n_{Ctrl}=15$, $n_{AD1}=15$, $n_{AD2}=20$, $n_{WT}=12$ mice. $^{*}p<0.05$; $^{**}p<0.01$ $^{***}p<0.001$; Data are shown as mean ± s.e.m.

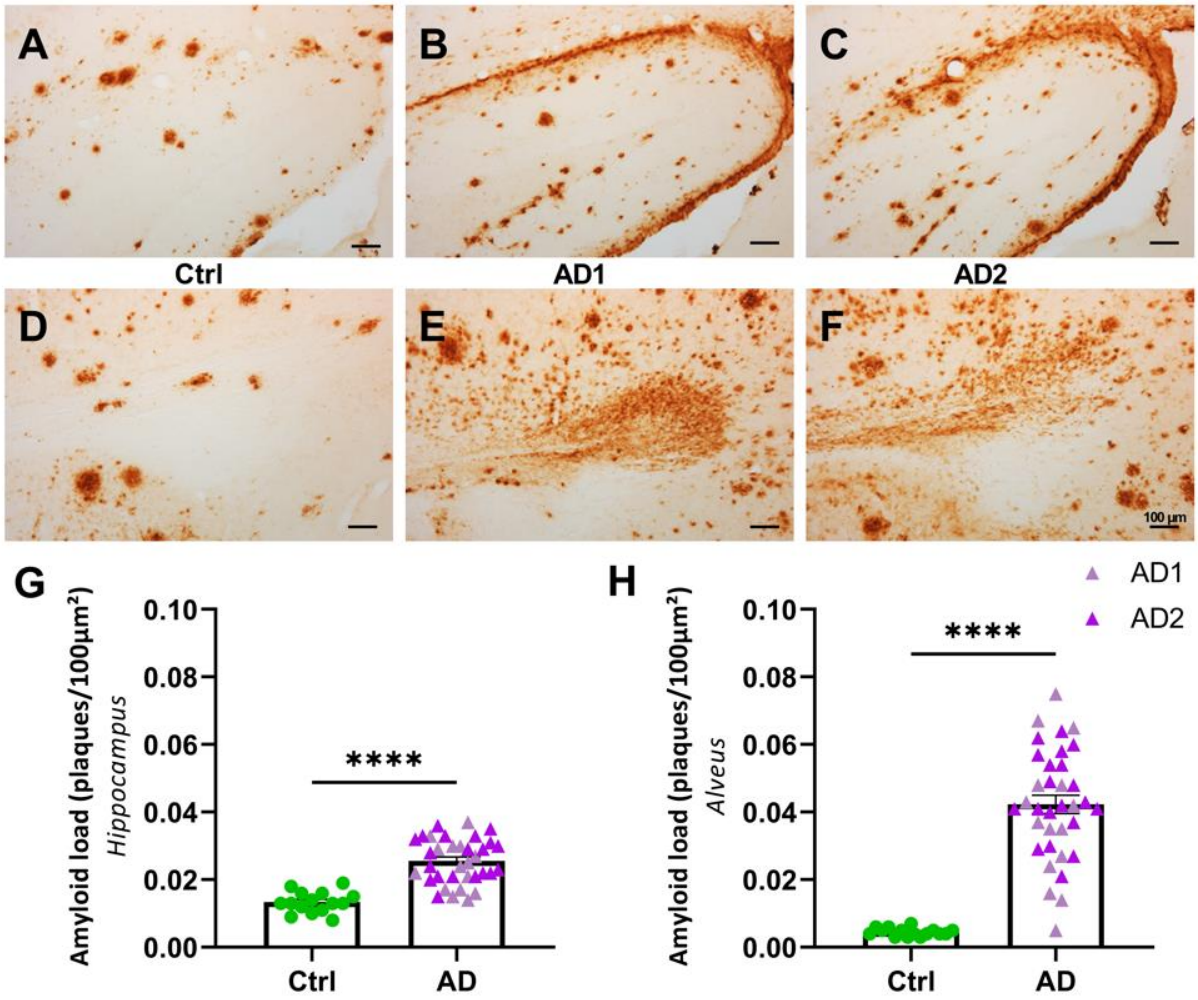

Figure 2. AD_{be} inoculation accelerates amyloidosis in $APP_{swe}/PS1_{dE9}$ mice close to the injection site. (**A-F**) Representative images of 4G8 immunolabelling showing Aβ pathology in the hippocampus (**A-C**) and alveus (**D-F**) of $APP_{swe}/PS1_{dE9}$ mice eight months after human brain inoculation. (**G-H**) Quantification of Aβ load (4G8-positive Aβ plaques per 100 µm²) revealed that AD_{be} inoculation accelerates Aβ deposition in the hippocampus (**G**, Mann Whitney's test, U=21.5, $p<0.0001$) and alveus (**H**, Mann Whitney's test, U=5, $p<0.0001$). ****$p<0.0001$. $n_{Ctrl}=15$, $n_{AD1}=15$, $n_{AD2}=20$ mice. Data are shown as mean ± s.e.m. Scale bars = 100 µm.

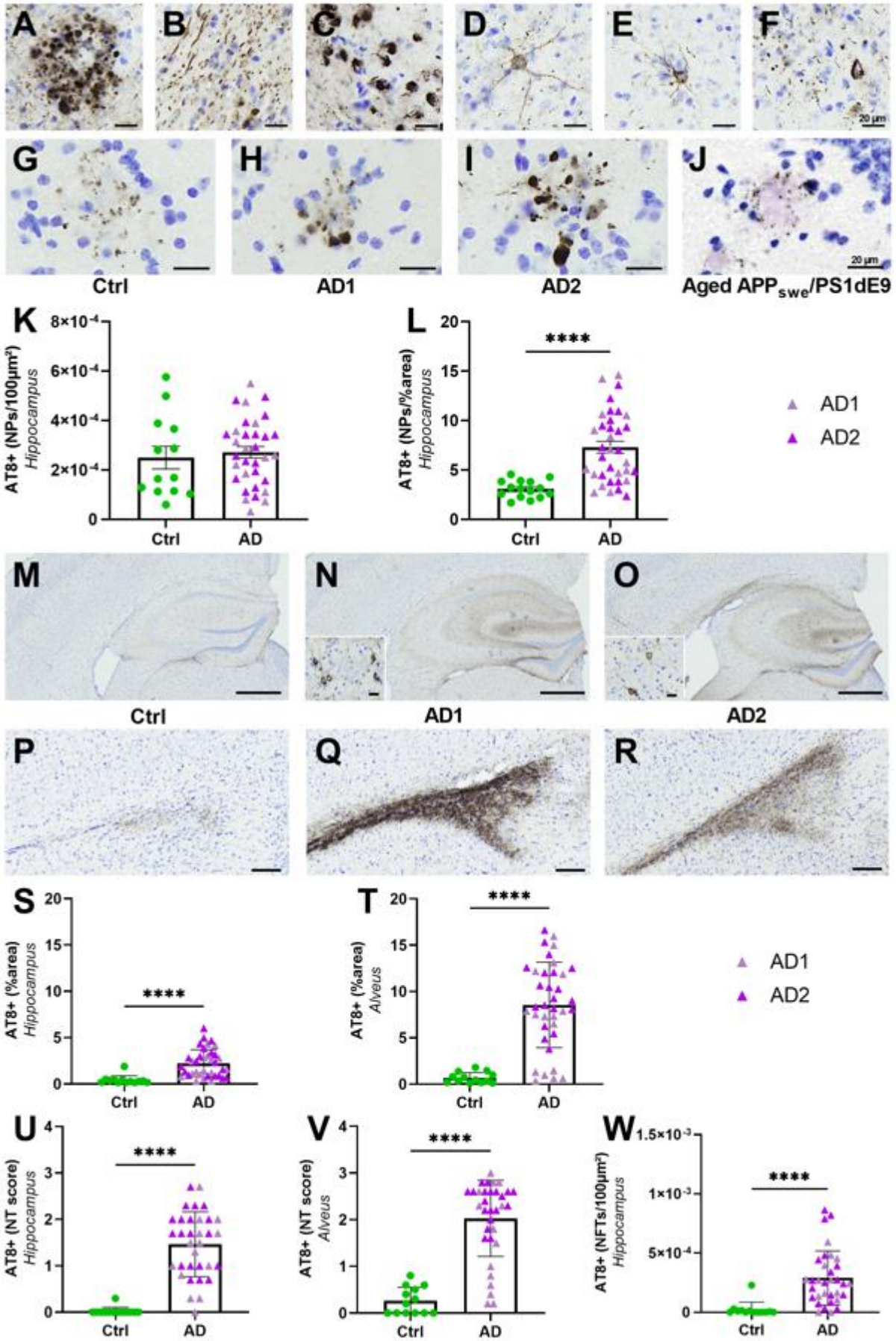
A
B
C
D
E
F
20 µm
G
H
I
J
20 µm
Ctrl
AD1
AD2
Aged APPswe/PS1dE9
K
AT8+ (NPs/100µm²)
Hippocampus
8×10⁻⁴
6×10⁻⁴
4×10⁻⁴
2×10⁻⁴
0
Ctrl
AD
L
AT8+ (NPs/%area)
Hippocampus
20
15
10
5
0
****
Ctrl
AD
AD1
AD2
M
N
O
Ctrl
AD1
AD2
P
Q
R
S
AT8+ (%area)
Hippocampus
20
15
10
5
0
****
Ctrl
AD
T
AT8+ (%area)
Alveus
20
15
10
5
0
****
Ctrl
AD
AD1
AD2
U
AT8+ (NT score)
Hippocampus
4
3
2
1
0
****
Ctrl
AD
V
AT8+ (NT score)
Alveus
4
3
2
1
0
****
Ctrl
AD
W
AT8+ (NFTs/100µm²)
Hippocampus
1.5×10⁻³
1×10⁻³
5×10⁻⁴
0
****
Ctrl
AD

847

Figure 3. AD_{be} inoculation induces tau pathology in $APP_{swe}/PS1_{dE9}$ mice around the injection site (8 mpi). AT8 immunolabelling revealed tau lesions in the forms of neuritic plaques (**A**), neuropil threads (**B**), NFTs (**C-F**). Representative images of AT8-positive neuritic plaques within the hippocampus of Ctrl- (**G**) and AD_{be}-inoculated (**H** for AD1, **I** for AD2) mice. AT8 immunolabelling of non-inoculated aged $APP_{swe}/PS1_{dE9}$ mice (24 months old) also revealed neuritic plaques (**J**). Quantification revealed similar neuritic plaque counts (NPs per 100 µm² of area) in all groups (**K**). The AT8-positive area within neuritic plaques (NP %area) was higher in AD_{be}- compared to $Ctrl_{be}$-inoculated animals suggesting that neuritic plaques were more tau-positive in the AD_{be} group (**L**, Mann Whitney's test, U=53.5, $p<0.0001$). (**M-R**) Representative images of AT8 immunolabelling showing tau pathology induction in the dorsal hippocampus (**M-O**) and alveus (**P-R**). Quantification of overall AT8-labelled phospho-tau (percentage of AT8-positive area), neuropil thread (NT) scoring and/or NFTs accumulation (AT8-positive NFTs per 100 µm² of area) in the hippocampus (**S, U, W. S**: $p<0.0001$. **U**: $p<0.0001$. **W**: $p<0.0001$; Mann Whitney's tests) and alveus (**T, V. T**: $p<0.0001$. **V**: $p<0.0001$; Mann Whitney's tests) showed an increase in tau pathology following AD_{be} inoculation compared to $Ctrl_{be}$. ****$p<0.0001$. $n_{Ctrl}=15$, $n_{AD1}=15$, $n_{AD2}=20$ mice. Data are shown as mean ± s.e.m. Scale bars = 20 µm (**A-J** and inserts), 500 µm (**M-O**) and 100 µm (**P-R**). NP = neuritic plaques; NT = neuropil threads; NFT = neurofibrillary tangles.

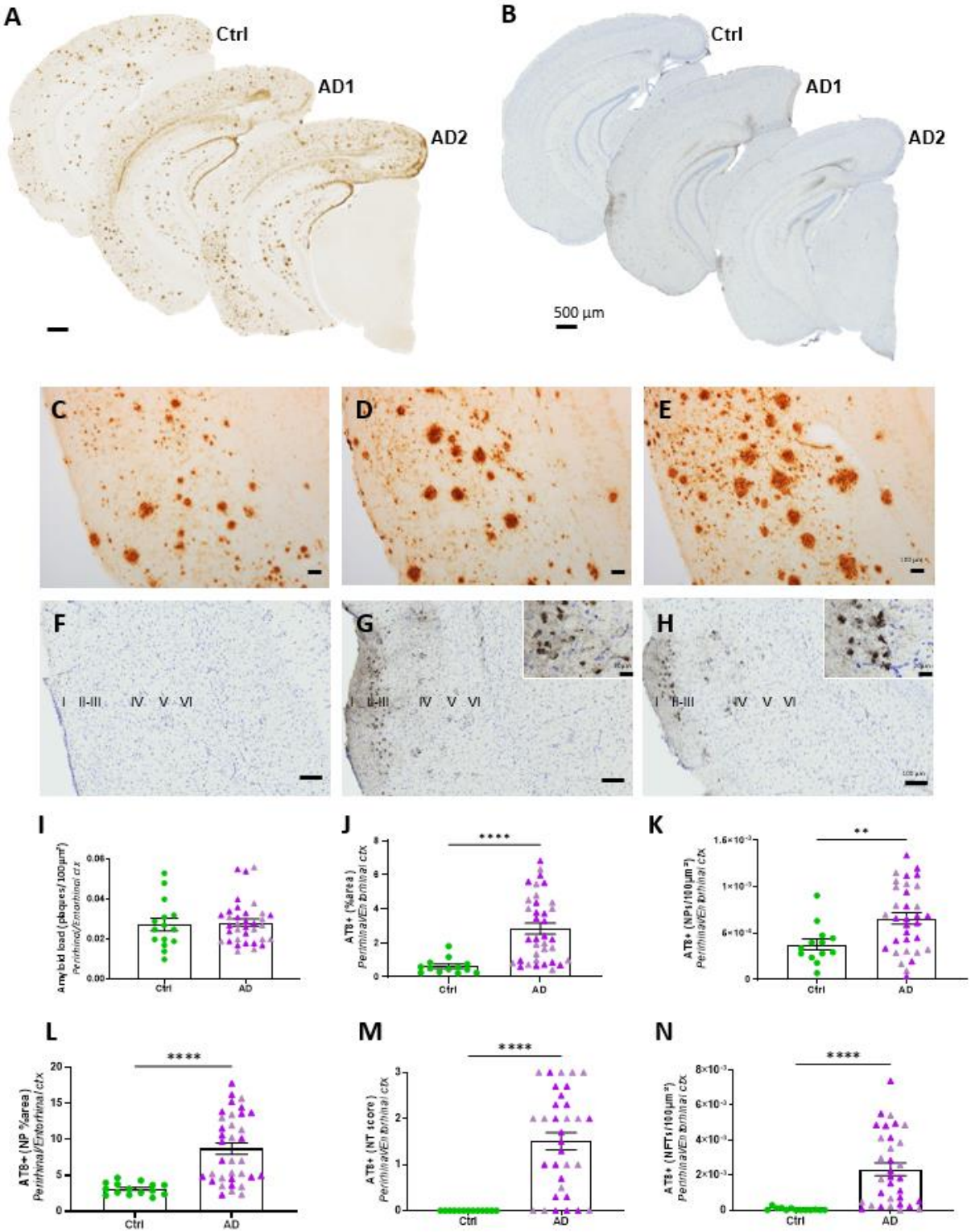

Figure 4. Aβ and tau pathologies in the perirhinal/entorhinal cortex following AD_{be} inoculation in $APP_{swe}/PS1_{dE9}$ mice. Representative images of the 4G8 immunolabelling showing Aβ pathology (**A**) and the AT8 immunolabelling showing tau pathology (**B**) in AD_{be}-inoculated $APP_{swe}/PS1_{dE9}$ mice. Magnified views of Aβ (**C-E**) and tau (**F-H**) lesions in the

perirhinal/entorhinal cortex. Quantification of Aβ load (**I**: $p>0.05$), overall AT8-positive tau lesions (**J**: $p<0.0001$), neuritic plaque (NPs) count (**K**: $p=0.0098$), AT8-positive area stained within neuritic plaques (**L**: $p<0.0001$), neuropil thread (NTs – **M**: $p<0.0001$), and NFTs (**N**: $p<0.0001$) in the perirhinal/entorhinal cortex. Mann Whitney's tests. **$p<0.01$; ****$p<0.0001$. $n_{Ctrl}=15$, $n_{AD1}=15$, $n_{AD2}=20$ mice. Data are shown as mean ± s.e.m. Scale bars = 500 µm (**A**-**B**), 100 µm (**C**-**H**) and 20 µm in inserts.

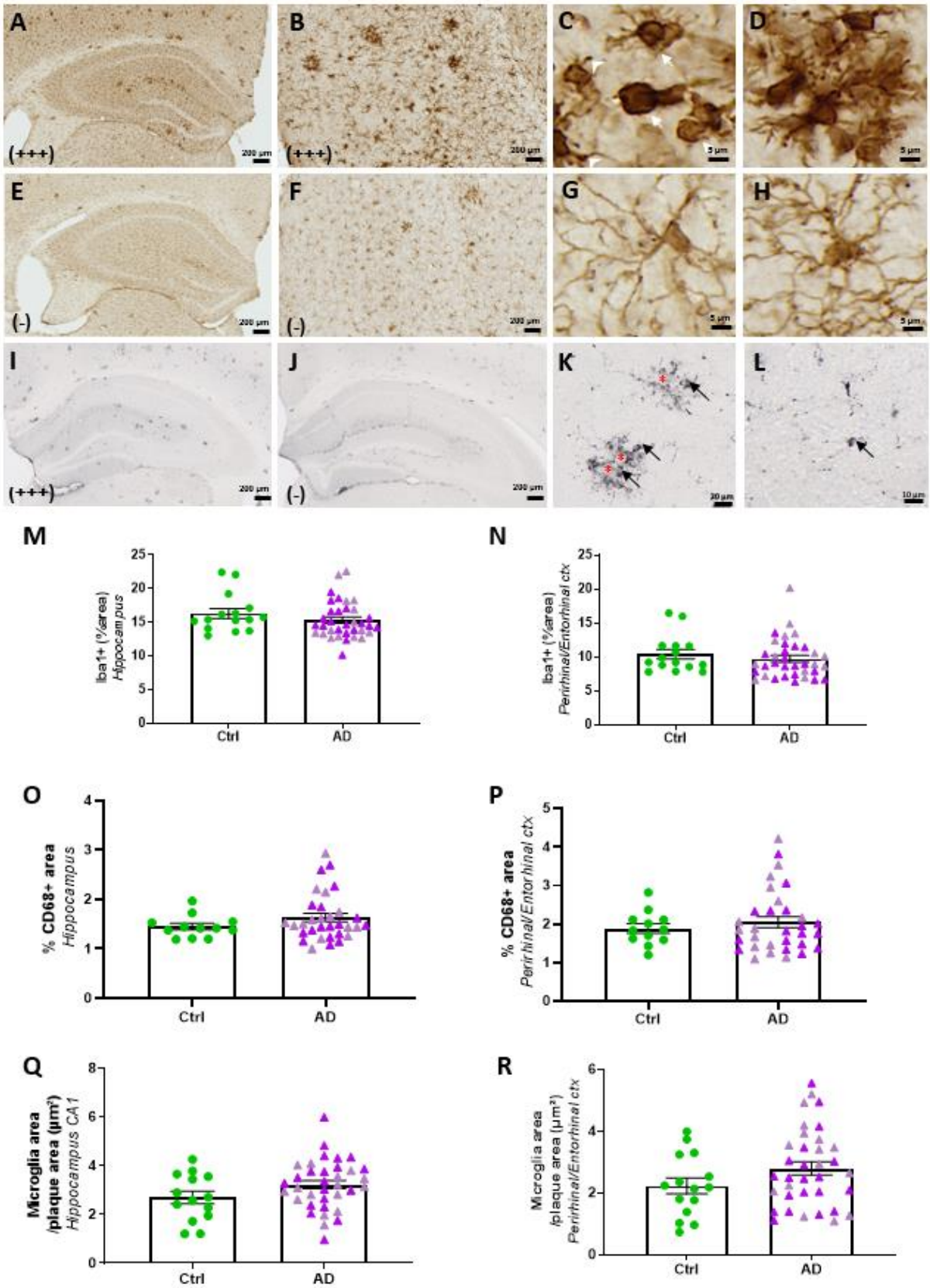

Figure 5. Microglial activation in AD_{be} and $Ctrl_{be}$-inoculated $APP_{swe}/PS1_{dE9}$ mice. Within each group, animals with high and low Iba1 staining were identified. Representative images of

one animal with higher Iba1 levels showing abundant staining in the hippocampus (**A**) and perirhinal/entorhinal cortex (**B**). Animals with higher Iba1 levels displayed activated microglia characterized by beading with spheroidal swellings of the processes and enlarged cell body with dystrophic ramifications (**C**, arrows). These activated cells formed microglial clusters surrounding Aβ plaques (**D**). Animals with lower Iba1 levels (**E-F**) displayed more cells with a highly ramified profile close to Aβ plaques (**G**) or far from plaques (**H**), consistent with a non-activated phenotype. Representative images of one animal with higher (**I**) or lower (**J**) CD68 staining in the hippocampus. Some clusters of CD68-stained microglia (arrows) surrounded Aβ deposits (*) (**K**) while some others were not associated with Aβ deposits (**L**). Similar levels of Iba1 (**M, N**) and CD68 (**O, P**) stained areas in the hippocampus or perirhinal/entorhinal cortex of Ctrl and AD animals (Mann Whitney's tests). Iba1-positive microglial load surrounding Aβ plaques was also similar in the different groups in both regions (**Q-R**, Mann Whitney's tests). n_{Ctrl}=15, n_{AD1}=15, n_{AD2}=20 mice.

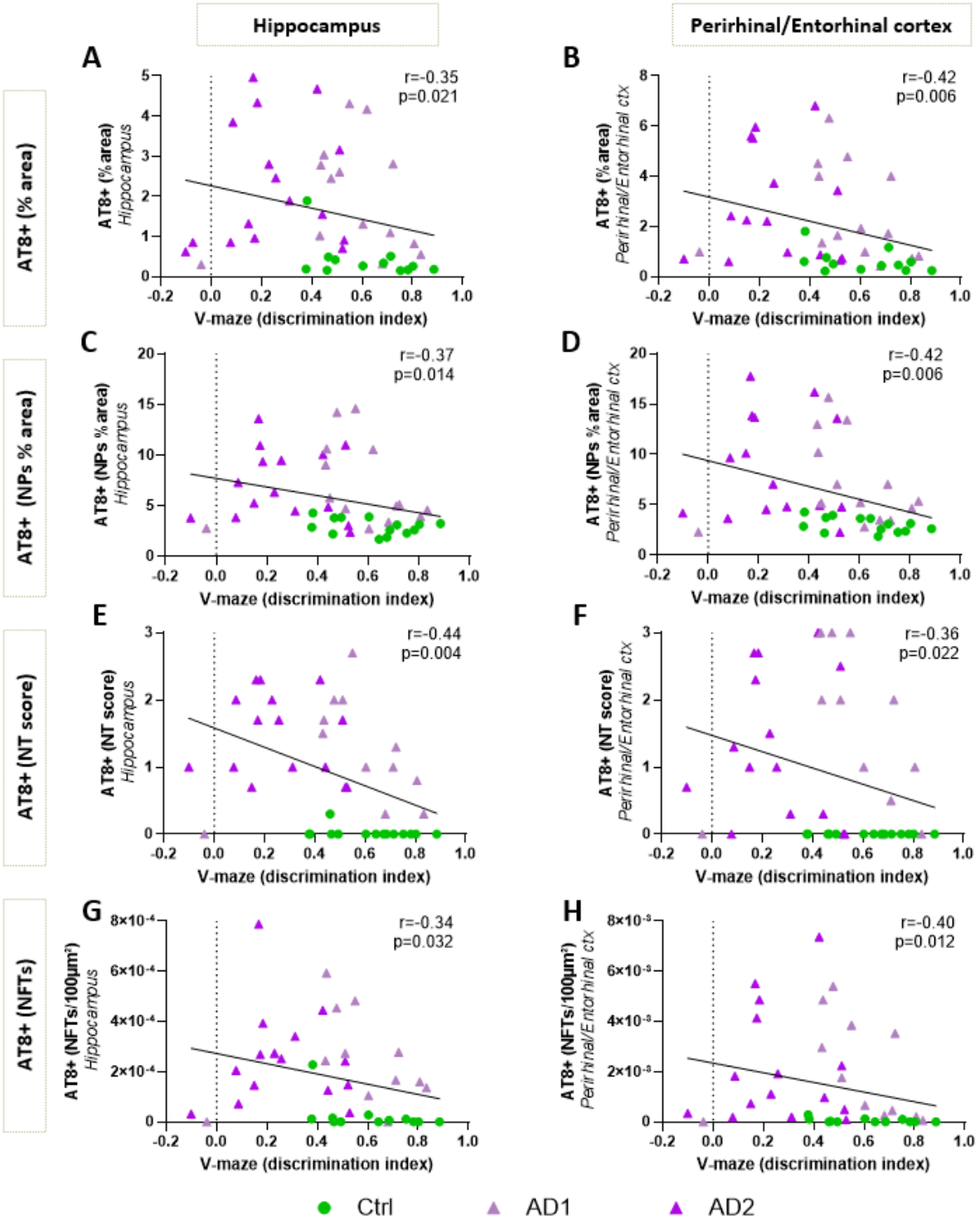

Figure 6. Inverse correlations between V-maze memory scores and tau lesions. V-maze memory scores (discrimination index) were inversely correlated with tau pathology both in the hippocampus and the perirhinal/entorhinal cortex. (**A-B**) Overall AT8-positive tau lesions. (**C-D**) AT8-positive area stained within neuritic plaques. (**E-F**) Neuropil threads (NT). (**G-H**)

Neurofibrillary tangles (NFTs). Spearman's correlations with significance level at $p<0.05$. $n_{Ctrl}=15$, $n_{AD1}=15$, $n_{AD2}=20$ mice.

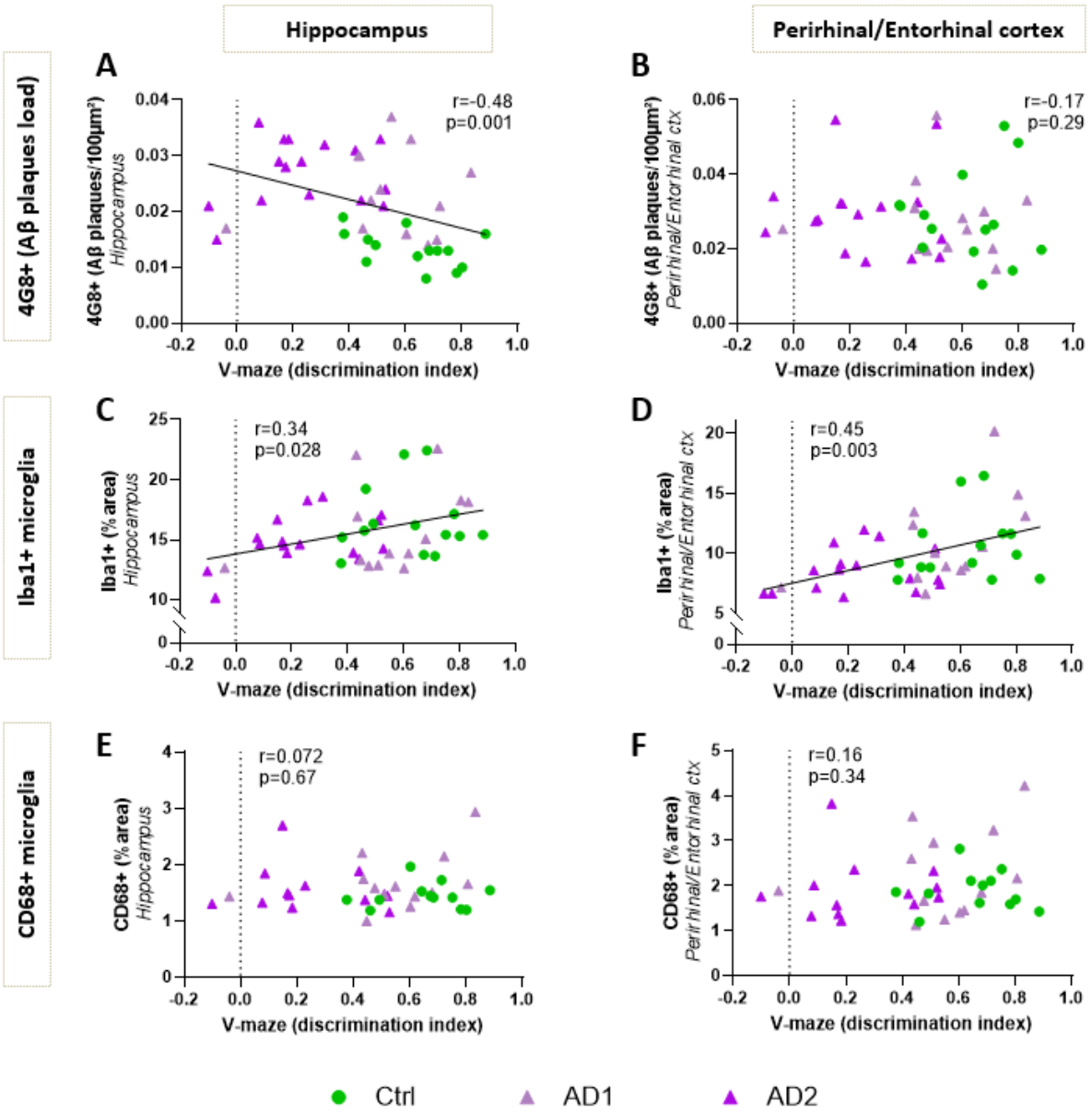

Figure 7. Correlations between V-maze memory scores and Aβ or microgliosis. V-maze memory scores (discrimination index) were inversely correlated with Aβ pathology in the hippocampus (**A**) but not in the perirhinal/entorhinal cortex (**B**). Microglial Iba1-positive staining was positively correlated with memory scores in both regions (**C-D**). Microglial CD68-positive staining was however not correlated with memory scores in either region (**E-F**). Spearman's correlations with significance level at $p<0.05$. $n_{Ctrl}=15$, $n_{AD1}=15$, $n_{AD2}=20$ mice.

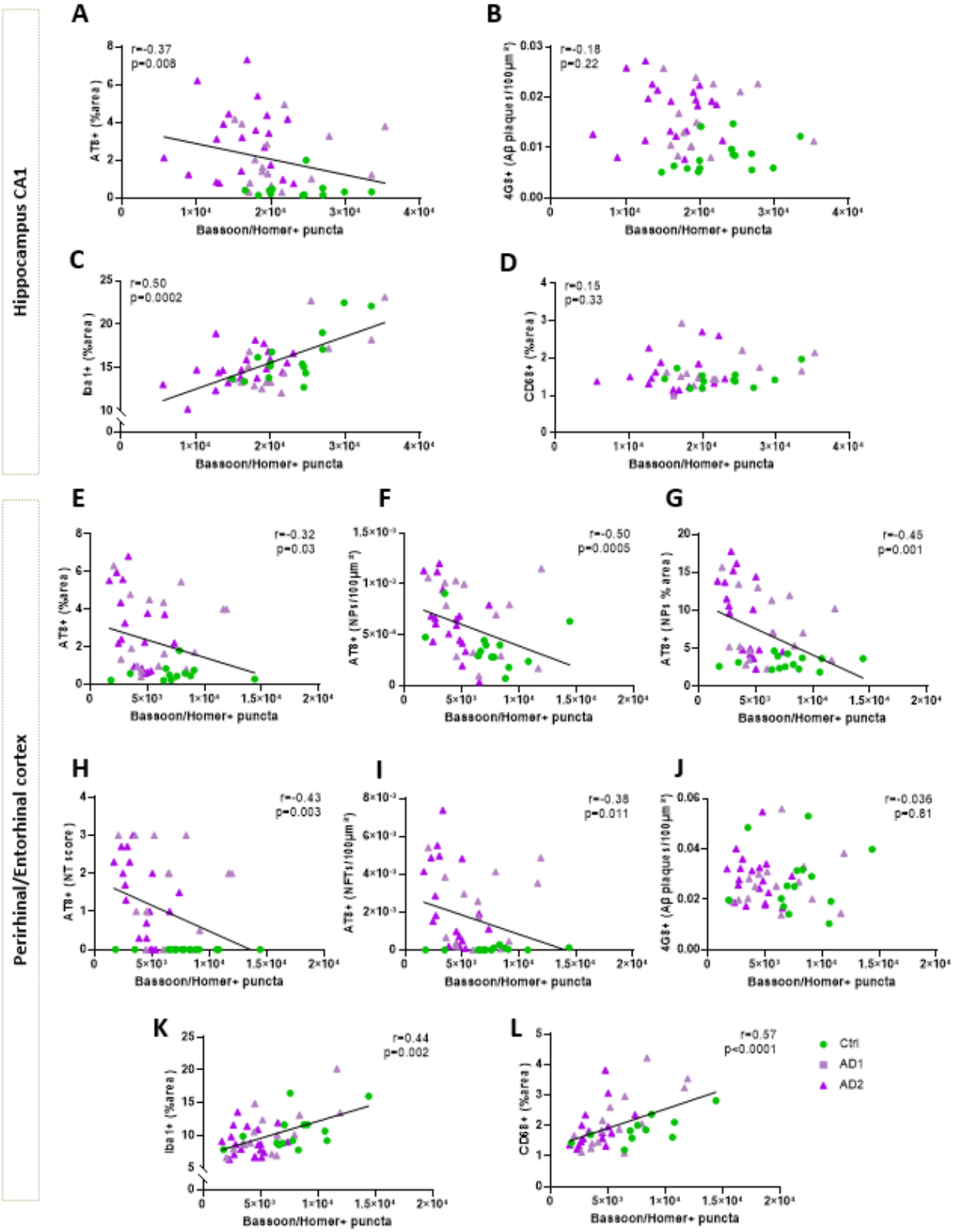

Figure 8. Correlations between synaptic density and tau lesions, Aβ plaque load or microglial activity. Synaptic density (Bassoon/Homer-positive puncta) was inversely

correlated with tau pathology both in the hippocampus (CA1) (**A**) and the perirhinal/entorhinal cortex (**E-I**), but not with Aβ pathology (**B, J**). Interestingly, synaptic density was positively correlated with microglial Iba1 labelling in the hippocampus (**C**) as well as in the perirhinal/entorhinal cortex (**K**). Microglial CD68 labelling in the perirhinal/entorhinal cortex (**L**), but not in the hippocampus (**D**) was correlated to synaptic density. Spearman's correlations with significance level at $p<0.05$. $n_{Ctrl}=15$, $n_{AD1}=15$, $n_{AD2}=20$ mice.

Links between memory, synapses, amyloid-beta, tau and microglial changes after tau pathology induction by Alzheimer's brain inoculation in amyloid-beta-plaque bearing mice

Supplementary data

Suzanne Lam, Anne-Sophie Hérard, Susana Boluda, Fanny Petit, Sabiha Eddarkaoui, Karine Cambon, The Brainbank Neuro-CEB Neuropathology Network, Jean-Luc Picq, Luc Buée, Charles Duyckaerts, Stéphane Haïk, Marc Dhenain

Supplementary Table 1. Patient characteristics.

Patient					Neuropathology						
ID	Age	Gender	Disease progression (months)	Post mortem delay (hours)	Braak stage	Thal stage	CAA	α-synuclein	TDP43	Hippocampal sclerosis	PrPSc
Ctrl1	66	M	-	26	II	0	0	0	0	0	0
Ctrl2	76	M	-	NA	II	0	0	0	0	0	0
AD1a	79	F	78	48.6	V	5	Type2	0	0	0	0
AD1b	87	F	72	29	V-VI	4	Type1	0	0	0	0
AD1c	89	F	96	30.6	V	5	Type1	0	0	0	0
AD1d	71	M	66	54	VI	4	Type2	Amygdala	0	0	0
AD2a	84	F	6	79	V	4	Type2	0	0	0	0
AD2b	81	F	36	NA	V	5	Type1	0	0	0	0
AD2c	81	F	36	26	VI	4	0	0	0	0	0
AD2d	86	F	36	20.5	V	4	Type2	0	0	0	0

Age-matched classical slowly (AD1) and rapidly evolving (AD2) Alzheimer patients were selected based on disease duration (over or under 36 months) and neuropathological evaluation, including similar Braak and Thal stages. Brains were negative for α-synuclein, TAR DNA-binding protein 43 (TDP43), hippocampal sclerosis and pathological prion PrPSc. Two non-Alzheimer control individuals (Ctrl) were also included in this study. NA: not available.

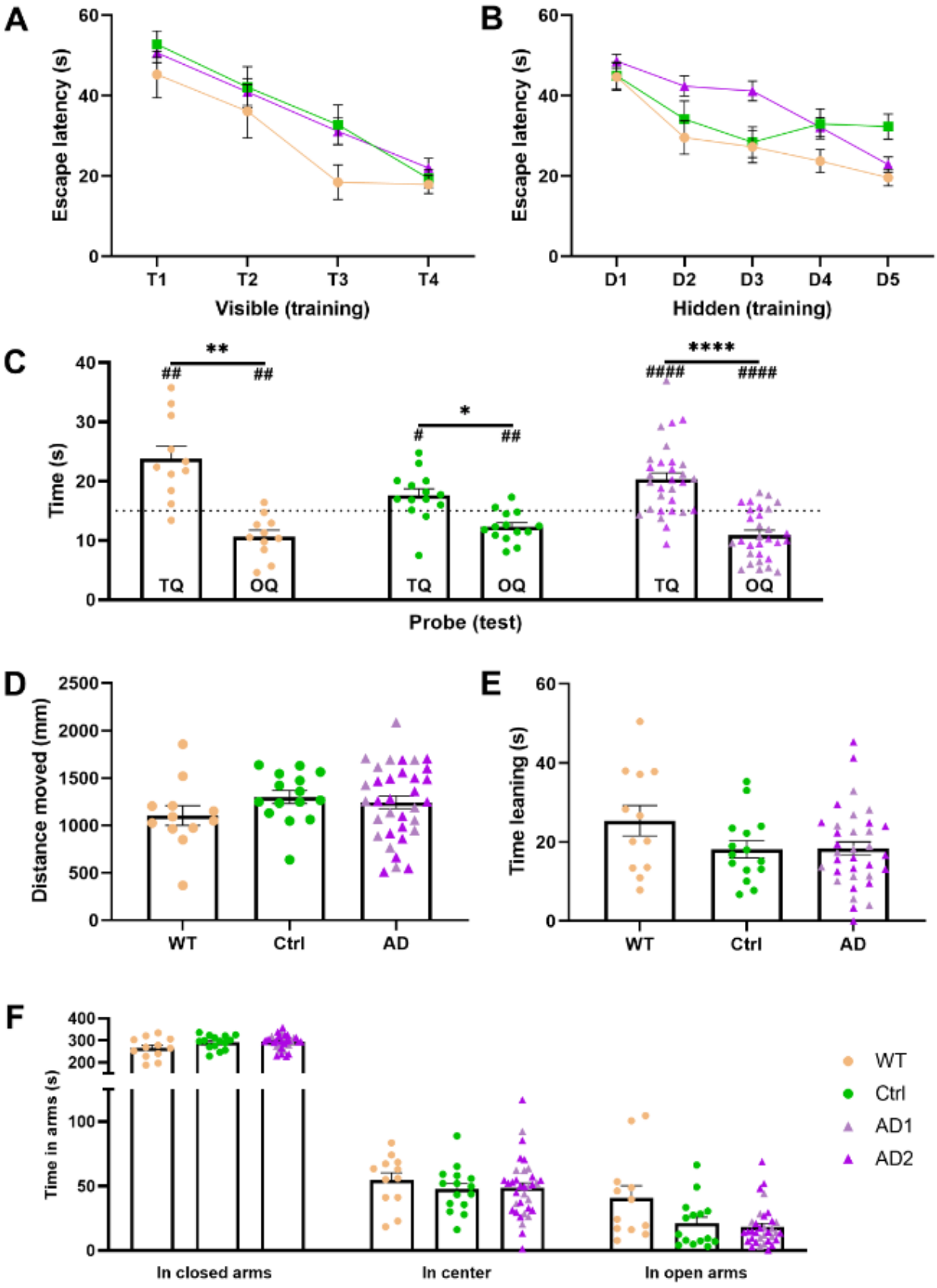
A
Escape latency (s)
60
40
20
0
T1
T2
T3
T4
Visible (training)
B
Escape latency (s)
60
40
20
0
D1
D2
D3
D4
D5
Hidden (training)
C
Time (s)
40
30
20
10
0
**
##
##
*
#
##
****
####
####
TQ
OQ
TQ
OQ
TQ
OQ
Probe (test)
D
Distance moved (mm)
2500
2000
1500
1000
500
0
WT
Ctrl
AD
E
Time leaning (s)
60
40
20
0
WT
Ctrl
AD
F
Time in arms (s)
400
300
200
100
50
0
In closed arms
In center
In open arms
WT
Ctrl
AD1
AD2

Supplementary Figure 1. AD_{be} and $Ctrl_{be}$-inoculated $APP_{swe}/PS1_{dE9}$ mice showed similar spatial memory performances and anxiety levels at 8 mpi. (**A-C**) Spatial memory was assessed using the Morris water maze test. During the visible platform phase (**A**), escape latencies steadily decreased across the four trials ($F_{(2.7, 139.8)}$=32.9, p<0.0001; two-way repeated measures ANOVA with the Geisser-Greenhouse correction and Dunnett's multiple comparisons). No difference was observed between the groups ($F_{(2, 52)}$=2.9, p=0.07; two-way repeated measures ANOVA with the Geisser-Greenhouse correction and Dunnett's multiple comparisons). For the hidden platform training phase (**B**), escape latencies were averaged across three trials per day and slowly decreased across the trials and days suggesting that mice had successfully learnt the platform position ($F_{(3.6, 187.5)}$=20.5, p<0.0001; two-way repeated measures ANOVA with the Geisser-Greenhouse correction and Dunnett's multiple comparisons). No difference was observed between the $Ctrl_{be}$ and AD_{be} groups suggesting that AD_{be} inoculations do not impact spatial learning abilities in $APP_{swe}/PS1_{dE9}$ mice after an eight-month incubation period ($F_{(1, 42)}$=1.6, p=0.22; two-way repeated measures ANOVA with the Geisser-Greenhouse correction and Dunnett's multiple comparisons). During the probe test evaluating spatial memory (**C**), the time spent in the target quadrant (TQ) was significantly higher than the time spent in the opposite one (OQ) (*p<0.05 for $Ctrl_{be}$-inoculated $APP_{swe}/PS1_{dE9}$ mice, **p<0.01 for WT mice, p<0.0001 for AD_{be}-inoculated $APP_{swe}/PS1_{dE9}$ mice; Tukey's multiple comparison test). Moreover, the time spent both in the TQ and OQ was significantly different from 15 seconds, which corresponds to 25% of the trial duration (## p<0.01; #### p<0.0001, one-sample Wilcoxon's signed-rank test). Spatial memory retention was evaluated after 72 hours. All groups performed as well as the $Ctrl_{be}$-inoculated WT group by spending more time in the target quadrant than in the opposite one, suggesting that memory is not impaired in $Ctrl_{be}$ or AD_{be}-inoculated $APP_{swe}/PS1_{dE9}$ mice (for the groups: $F_{(2, 52)}$=0.26, p>0.05; for TQ versus OQ: p=0.0028, p=0.0217, p<0.0001, respectively for WT, Ctrl, AD groups; two-way ANOVA with the Geisser-Greenhouse correction and Dunnett's multiple comparisons). (**D-F**) Anxiety levels

were assessed using the elevated plus maze. Comparable travelled distance (**D**), time spent leaning over the maze (**E**) and time spent in the different areas of the maze (open/closed arms and center of the maze) (**F**) were reported between the groups (p>0.05; Kruskal-Wallis' test with Dunn's multiple comparisons). n_{Ctrl}=15, n_{AD1}=15, n_{AD2}=20, n_{WT}=12 mice. Data are shown as mean ± s.e.m.

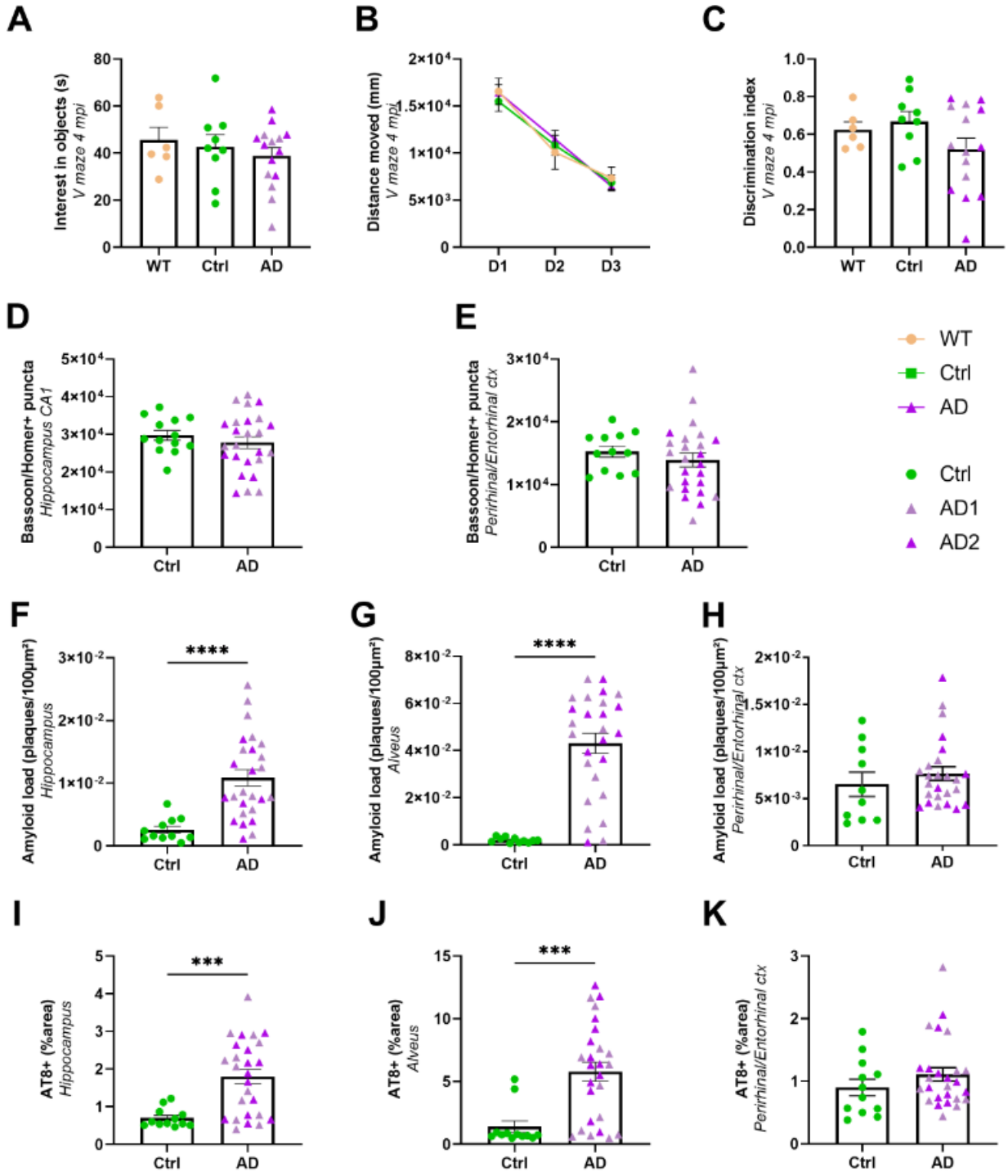

Supplementary Figure 2. Cognitive performance, synaptic density, Aβ and tau loads evaluations at 4 mpi. (**A-C**) Object recognition performances were evaluated at 4 mpi using a V-maze test. WT mice and $APP_{swe}/PS1_{dE9}$ mice inoculated with $Ctrl_{be}$ or AD_{be} had comparable exploratory activity, as suggested by the time spent on exploring the objects (**A**) (p>0.05; Kruskal-Wallis with Dunn's multiple comparisons) and the distance moved throughout the 3-day test (**B**) (for the days: $F_{(1.9, 51.7)}$=131.2, p<0.0001; for the groups: $F_{(2, 27)}$=0.06, p=0.9; two-way repeated measures ANOVA with the Geisser-Greenhouse correction and Dunnett's multiple comparisons). No difference in the novel object recognition test was reported between the groups, as similar discrimination indexes were observed (**C**) (p>0.05; Kruskal-Wallis with Dunn's multiple comparisons). (**D-E**) Quantification of Bassoon and Homer colocalization at 4 mpi did not show any differences in the CA1 (**D**) and in the perirhinal/entorhinal cortex (**E**) between the groups (p>0.05; Mann Whitney's test). (**F-H**) Aβ load quantification at 4 mpi revealed that AD_{be} inoculation accelerates Aβ deposition in the hippocampus (**F**) and alveus (**G**), but not the perirhinal/entorhinal cortex (**H**) (in the hippocampus p<0.0001, in the alveus p<0.0001, in the perirhinal/entorhinal cortex p=0.3; Mann Whitney's test). (**I-K**) AT8-positive tau overall quantification at 4 mpi revealed that AD_{be} inoculation induces tau lesions in the hippocampus (**I**), in the alveus (**J**) but not the perirhinal/entorhinal cortex (**K**) (p= 0.0007 in the hippocampus, p= 0.0003 in the alveus, p=0.2 in the perirhinal/entorhinal cortex; Mann Whitney's test). ***p<0.001; ****p<0.0001. n_{Ctrl}=9, n_{AD1}=7, n_{AD2}=8, n_{WT}=6 mice in A-C, n_{Ctrl}=11, n_{AD1}=14, n_{AD2}=12 in D-K. Data are shown as mean ± s.e.m.

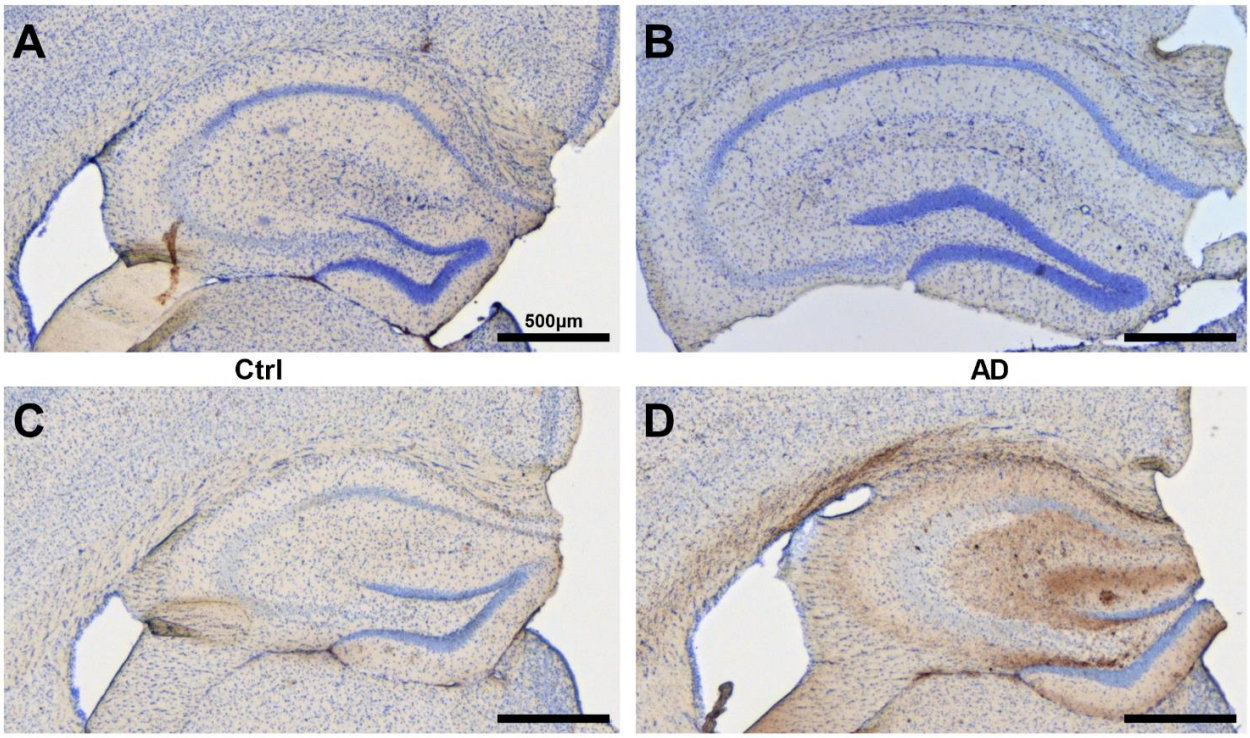

Supplementary Figure 3. AT8 immunolabelling in the hippocampus of Ctrl$_{be}$- (A, C) and AD$_{be}$-inoculated (B, D) APP$_{swe}$/PS1$_{dE9}$ mice at 1 mpi (A-B) and 8 mpi (C-D). AT8-positive tau lesions were not detected in 1 mpi APP$_{swe}$/PS1$_{dE9}$ mice (B) while they were detected at 8mpi (D).

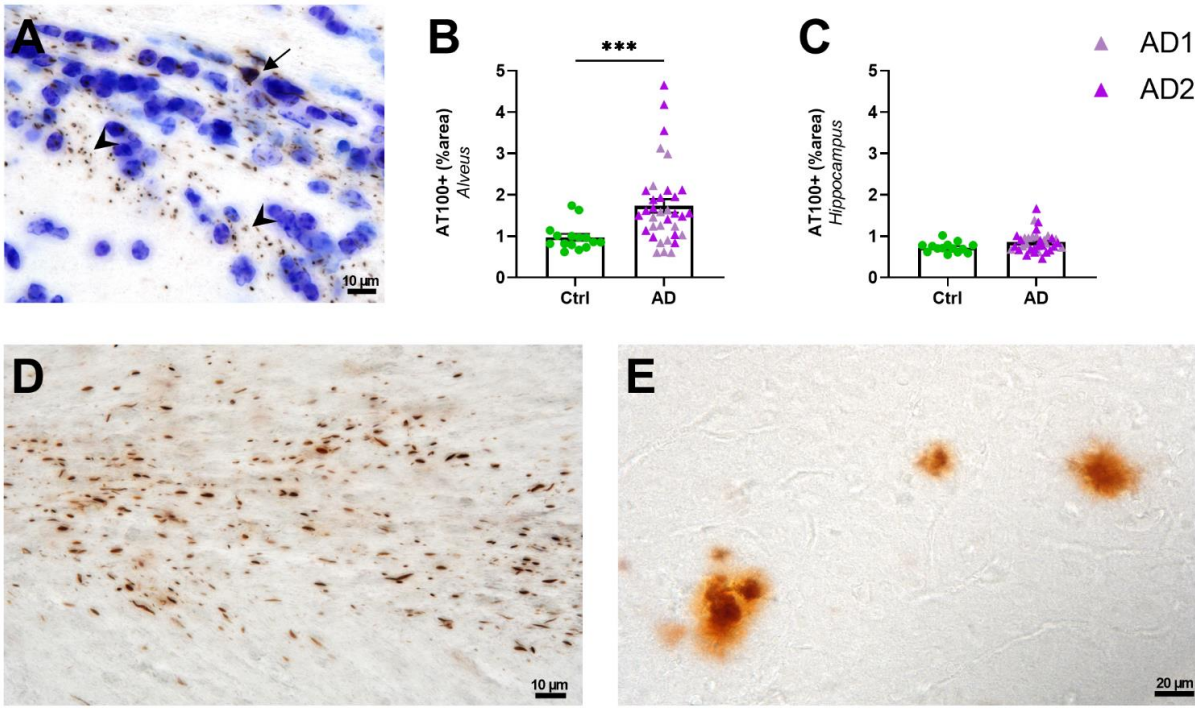

Supplementary Figure 4. AT100 and Gallyas-positive lesions next to the inoculation site of $APP_{swe}/PS1_{dE9}$ mice 8 months after AD_{be} infusion. (**A**) AT100 staining revealed NTs (arrowheads) and NFTs (arrow). (**B-C**) Overall quantification of AT100 labelling showed increased labelling in the alveus (**B**) and a trend for increased labelling in the hippocampus (**C**) of AD_{be}-inoculated mice (p=0.0007 and 0.092 respectively, Mann-Whitney test). Gallyas silver staining revealed neuropil threads (**D**) as well as Aβ plaques (**E**) in AD_{be}-inoculated mice. n_{Ctrl}=15, n_{AD1}=15, n_{AD2}=20. Data are shown as mean ± s.e.m. Scale bars = 10 µm (**A, D**) and 20 µm (**E**).

942

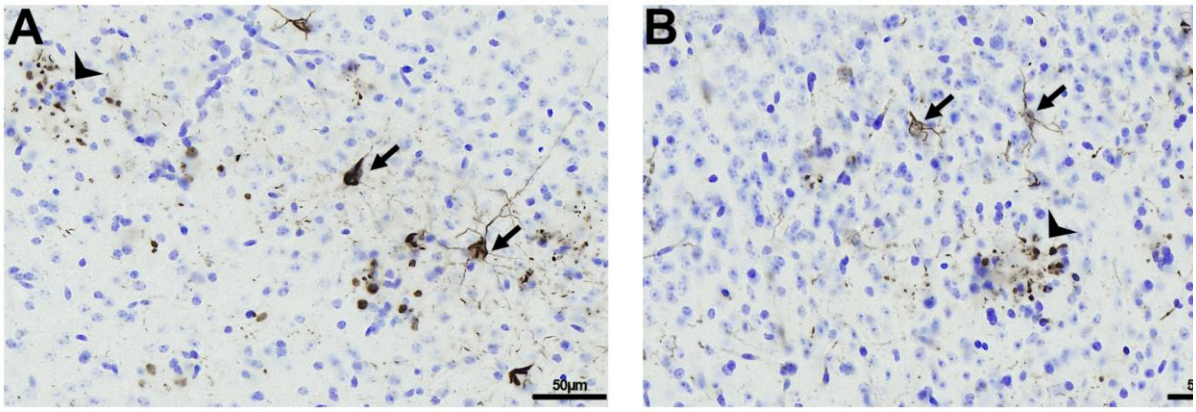

Supplementary Figure 5. AT8-positive lesions in the visual cortex of $APP_{swe}/PS1_{dE9}$ mice 8 months after AD_{be} infusion. AT8 staining revealed NFTs (arrows) surrounded by neuropil threads, as well as neuritic plaques (arrowheads), in the visual cortex of AD1 (**A**) and AD2 (**B**) brain-inoculated mice. Scale bars = 50 µm.

943

944

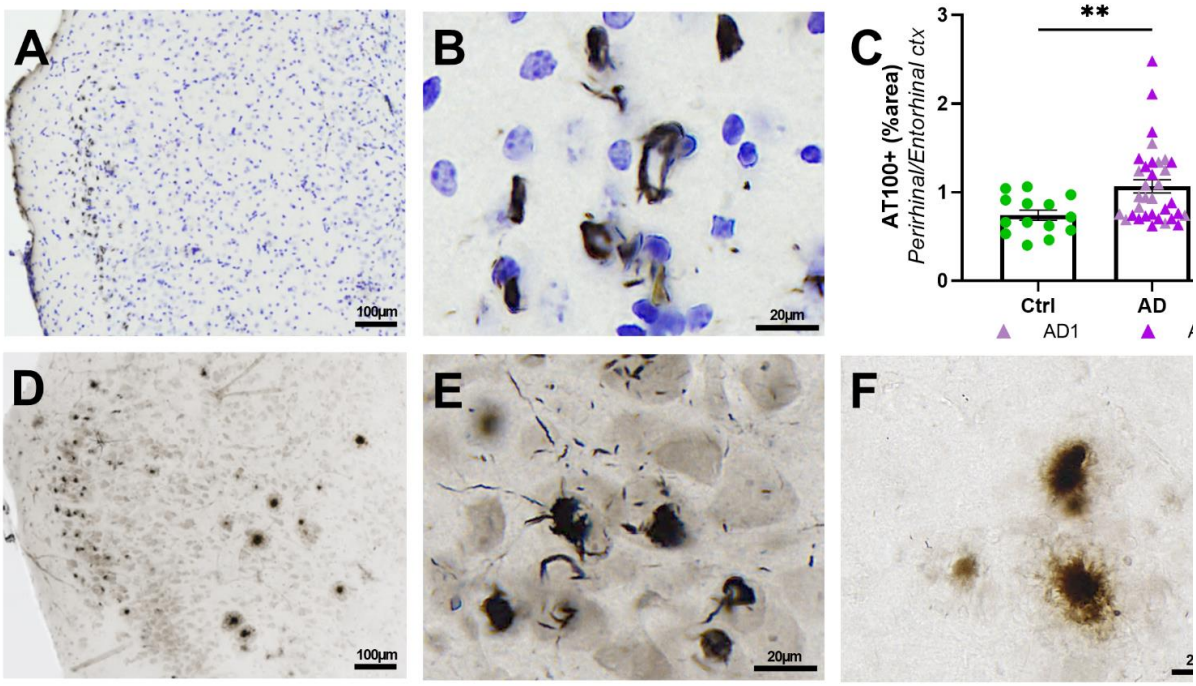

Supplementary Figure 6. AT100- and Gallyas-positive lesions spreading to the perirhinal/entorhinal cortex of APP$_{swe}$/PS1$_{dE9}$ mice 8 months after AD$_{be}$ infusion. (**A-B**) AT100 staining revealed NFTs in the perirhinal/entorhinal cortex. (**C**) Overall quantification of AT100 labelling showed increased labelling in the perirhinal/entorhinal cortex of AD$_{be}$-inoculated mice compared to Ctrl$_{be}$-inoculated ones (p=0.005, Mann-Whitney test). (**D-F**) Gallyas silver staining revealed labelled neurons evoking NFTs (**E**) as well as Aβ plaques (**F**). n_{Ctrl}=15, n_{AD1}=15, n_{AD2}=20. Data are shown as mean ± s.e.m. Scale bars = 100 µm (**A, D**) and 20 µm (**B, E, F**).

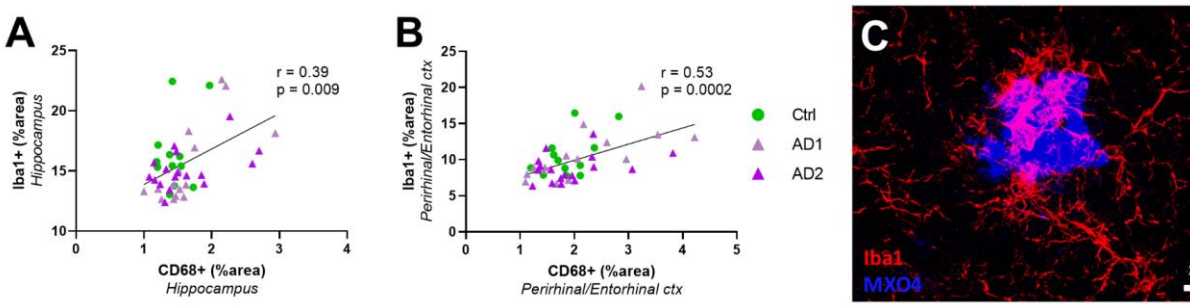

Supplementary Figure 7. Iba1 and CD68 staining. Iba1 staining level was correlated with CD68 labelling in the hippocampus (**A**) and in the perirhinal/entorhinal cortex (**B**). Confocal microscopy of Iba1-positive microglia (red) surrounding Aβ deposition stained by MXO4 (blue) (**C**). Scale bar = 20µm.

947

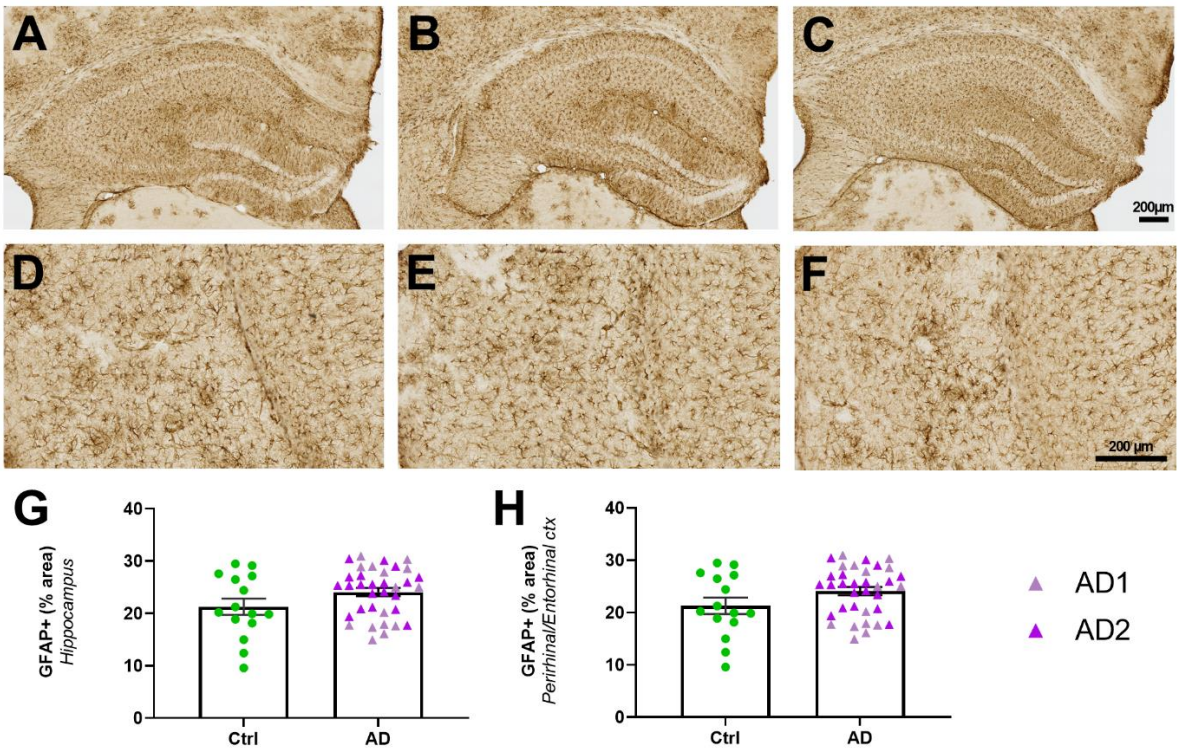

Supplementary Figure 8. Astrocytic coverage was similar in the hippocampus and perirhinal/entorhinal cortex of AD_{be}- and $Ctrl_{be}$-inoculated $APP_{swe}/PS1_{dE9}$ mice at 8 mpi. GFAP staining revealed similar astrocytic loads in the hippocampus (**A-C, G**) and perirhinal/entorhinal cortex (**D-F, H**) of AD_{be}- and $Ctrl_{be}$-inoculated $APP_{swe}/PS1_{dE9}$ mice at 8 mpi. n_{Ctrl}=15, n_{clAD}=15, n_{rpAD}=20 mice. Data are shown as mean ± s.e.m. Scale bars = 200 µm.

948

949

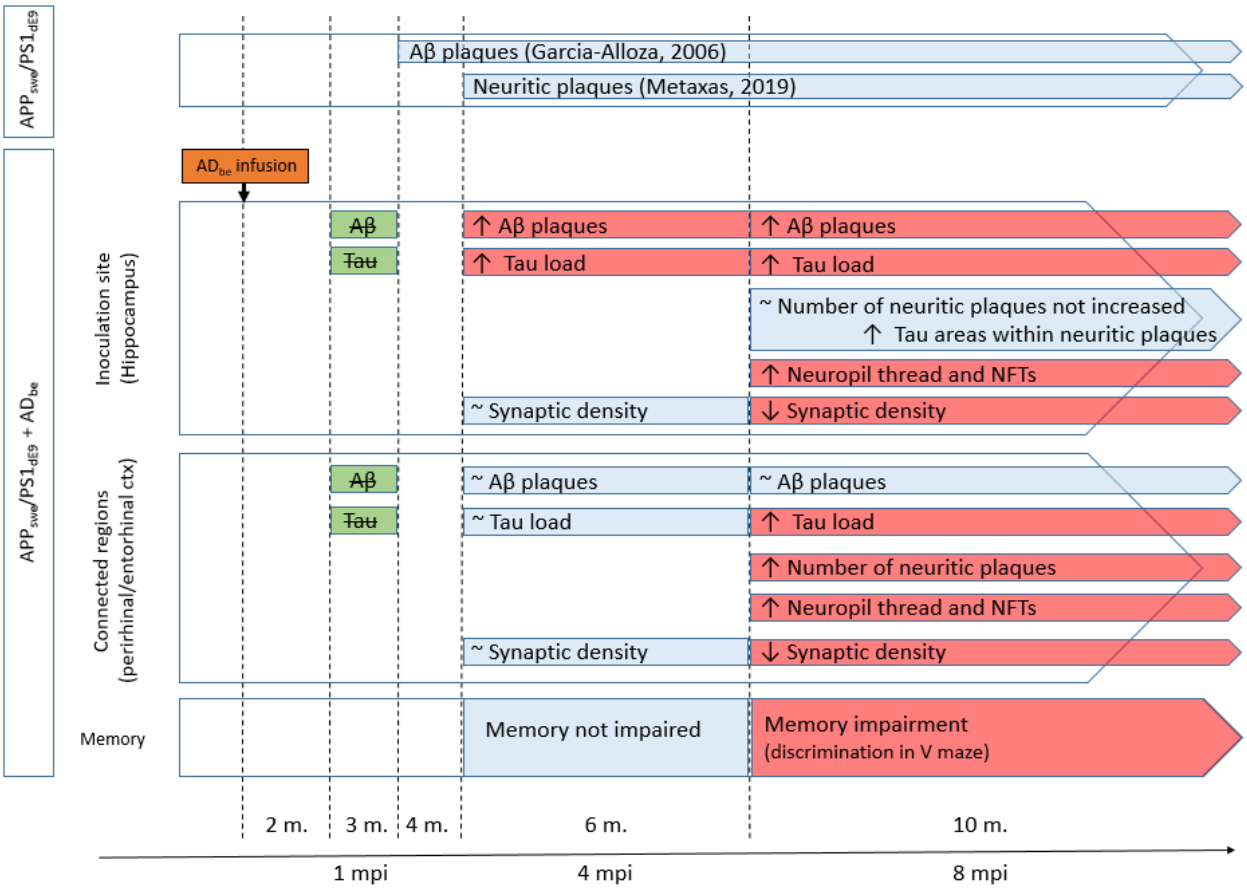

Supplementary Figure 9. Overview of the changes reported after infusion of AD_{be} in $APP_{swe}/PS1_{dE9}$. The first lines ($APP_{swe}/PS1_{dE9}$) display published timeframe for occurrence of Aβ plaques (4 month of age) and tau-positive neuritic plaques (6 months of age) in $APP_{swe}/PS1_{dE9}$ mice. The lines below ($APP_{swe}/PS1_{dE9}$+AD_{be}) display events reported in AD_{be}-inoculated $APP_{swe}/PS1_{dE9}$ mice compared to $Ctrl_{be}$-inoculated $APP_{swe}/PS1_{dE9}$ animals. One month post inoculation (mpi), Aβ and tau were not detected in AD_{be}-inoculated $APP_{swe}/PS1_{dE9}$ mice. Blue frames display events that were similar in AD_{be}- and Ctrlbe-inoculated $APP_{swe}/PS1_{dE9}$ animals. Red frames highlight impairments detected in AD_{be}-inoculated $APP_{swe}/PS1_{dE9}$ mice. First changes occurred within the hippocampus 4 mpi. Synaptic density and memory were not modified at this stage. Then at 8 mpi, changes continued to involve the hippocampus and extended to connected regions (perirhinal/entorhinal cortex). Synaptic density was reduced and memory was impaired at this stage.

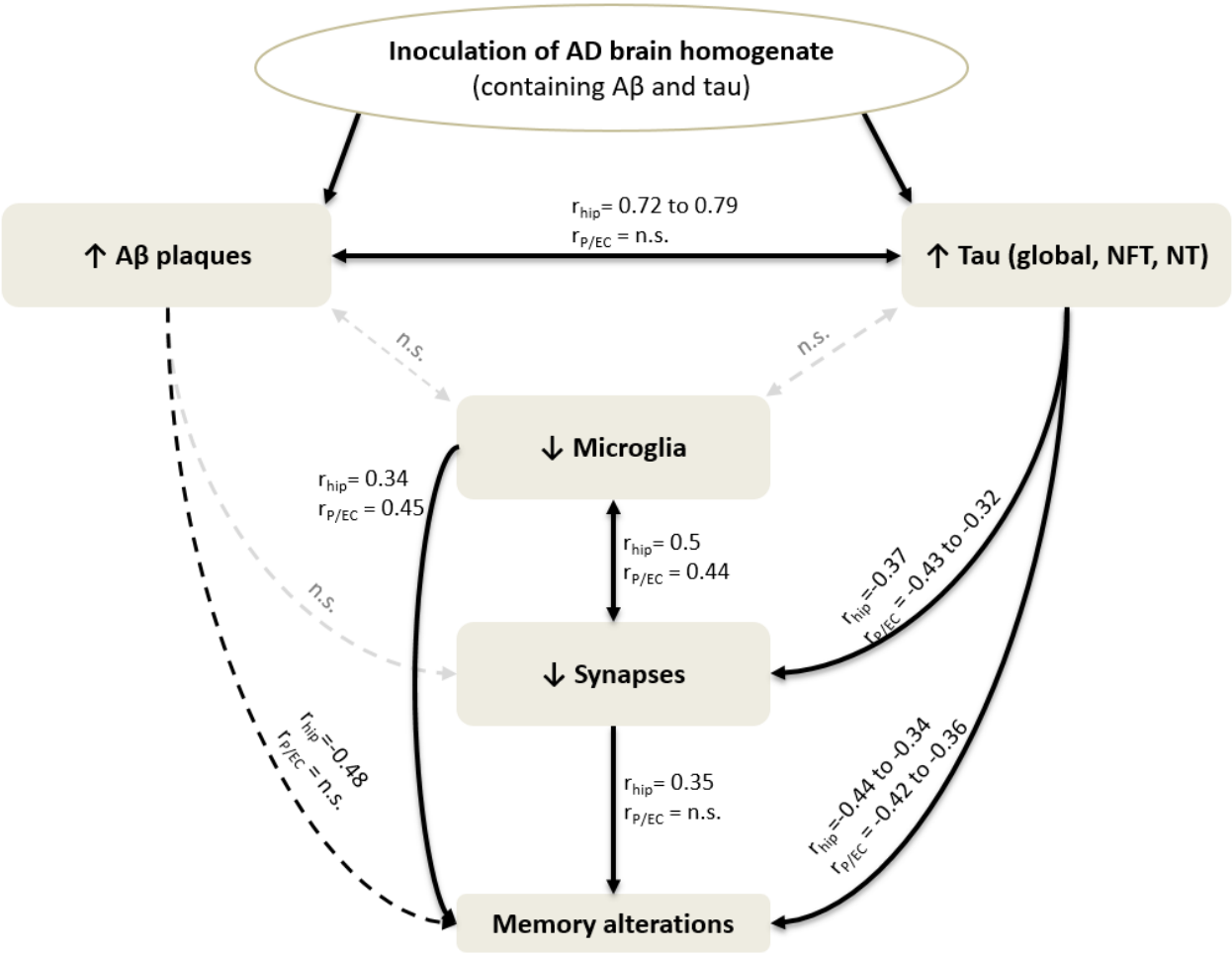

Supplementary Figure 10. Overview of correlation coefficients between Aβ plaques, tau aggregates, microglia, memory scores, and synaptic markers. The inoculation of AD_{be} accelerates Aβ deposition locally and induces tau lesions in $APP_{swe}/PS1_{de9}$ mice. The severity of tau (but not Aβ) lesions and reduced microglial loads were correlated with memory alterations and with synaptic loss. Spearman correlations with a significance level set at 0.05.